



## OPEN ACCESS

## EDITED BY

Wupeng Xiao,  
Xiamen University, China

## REVIEWED BY

Daniela Ruberti,  
University of Campania Luigi Vanvitelli, Italy  
Chao Zhan,  
Ludong University, China

## \*CORRESPONDENCE

Wei Gao

✉ gaoweigeo@fio.org.cn

†These authors share first authorship

RECEIVED 04 September 2024

ACCEPTED 06 December 2024

PUBLISHED 06 January 2025

## CITATION

Yang Z, Gao W, Yu W, Liu J, Du J, Li P, Xu Y and Li P (2025) The spatiotemporal changes and influencing mechanisms of the coastline in the Yellow River Delta, China.  
*Front. Mar. Sci.* 11:1490990.  
doi: 10.3389/fmars.2024.1490990

## COPYRIGHT

© 2025 Yang, Gao, Yu, Liu, Du, Li, Xu and Li. This is an open-access article distributed under the terms of the [Creative Commons Attribution License \(CC BY\)](https://creativecommons.org/licenses/by/4.0/). The use, distribution or reproduction in other forums is permitted, provided the original author(s) and the copyright owner(s) are credited and that the original publication in this journal is cited, in accordance with accepted academic practice. No use, distribution or reproduction is permitted which does not comply with these terms.

# The spatiotemporal changes and influencing mechanisms of the coastline in the Yellow River Delta, China

Zhuo Yang<sup>1†</sup>, Wei Gao<sup>1,2\*†</sup>, Wenjie Yu<sup>1</sup>, Jie Liu<sup>1,2</sup>, Jun Du<sup>1,3</sup>, Ping Li<sup>1,3</sup>, Yuanqin Xu<sup>1,2</sup> and Ping Li<sup>1,2</sup>

<sup>1</sup>Key Laboratory of Marine Geology and Metallogeny, First Institute of Oceanography, Ministry of Natural Resources (MNR), Qingdao, China, <sup>2</sup>Laboratory for Marine Geology, Qingdao Marine Science and Technology Center, Qingdao, China, <sup>3</sup>Research Center for Coastal Zone Science and Marine Development Strategy, First Institute of Oceanography, Ministry of Natural Resources (MNR), Qingdao, China

Using remote sensing imagery of the Yellow River Delta (YRD) from 1984 to 2024, the Digital Shoreline Analysis System (DSAS) model was employed to analyze the coastline position, migration rate, and characteristics of four typical coastal sections. The response of the coastline changes in the study area to global climate change and human activities was quantitatively assessed. Over the past 40 years, the modern YRD coastline has generally advanced seaward at an average rate of 109.64 m/a. This progression can be divided into three distinct phases: (i) The rapid transition period from 1984 to 2000, during which the total coastline length reached its maximum of nearly 440.65 km in the last 40 years. In 1986, the proportion of artificial coastline surpassed that of natural coastline for the first time. (ii) A decreasing trend in total coastline length characterized the slow transition period from 2000 to 2015. The transition in coastline types continued the trend of the previous period, with artificial coastlines exceeding 90% for the first time in 2015, marking the highest proportion in the past 40 years. (iii) The stable period from 2015 to the present, during which the total coastline length has shown an increasing trend. The artificial coastline has stabilized, while the growth of the natural coastline has been concentrated around the Yellow River estuary. However, the increase in the natural coastline has gradually slowed due to water and sediment regulation projects from 2001. The evolution of the coastline in the YRD has shifted from early control by river diversions to a current primary influence from human-driven land reclamation projects. Coastal changes in the present estuarine sections are mainly controlled by Yellow River water and sediment inflows, while abandoned northern channels experience pronounced effects from extreme weather, such as cold wave-induced winds. Additionally, factors such as sea-level rise due to global climate change and delta subsidence caused by sediment compaction have lowered the relative elevation of the coastline, further accelerating its erosion and retreat. However, these natural factors have had a lesser impact on coastline evolution than river diversions and human activities.

## KEYWORDS

Yellow River Delta, remote sensing, digital shoreline analysis system, coastline changes, human activity

# 1 Introduction

Deltas are continuous sedimentary formations deposited both above and below water as rivers flow into basins (Avornyo et al., 2023; Nguyen et al., 2023), representing the interaction between rivers and oceans (Gao, 2011; Li P. et al., 2023; Higgins, 2016). Deltas serve as transitional zones between land and sea, situated at the boundary between terrestrial and marine environments (Wang et al., 2005). They accumulate large volumes of sediment, carrying rich terrestrial material and transporting some of these sediments into deeper marine areas. Thus, they play a crucial role in sediment transport's "Source-Sink" process from land to sea (Ji et al., 2022). As major global economic centers and population hubs (Edmonds et al., 2020), deltas are not only the cradles of human civilization but also possess significant ecological value and abundant natural resources (Bianchi et al., 2016). Therefore, the sustainable development of deltas has emerged as a primary priority for future growth.

As a critical component of the delta coastal zone, the coastline separates land from water and serves as a key element in studying environmental evolution in deltas. It is also crucial for measuring and calculating terrestrial and water resources. Changes in the coastline significantly impact the ecological environment, port operations, transportation safety, and the utilization of coastal land resources (Ye et al., 2016). Significant disparities exist in the intensity of coastline development among the world's major deltas, leading to varying trends in coastline changes. For instance, the Yangtze River Delta has experienced an average annual coastline increase of 74.6 km over the past 30 years; the Pearl River Delta saw its coastline length increase by nearly 100 km from 1990 to 2019 (Liu Y. et al., 2023); the modern coastline of the Mississippi River Delta has stabilized, with only localized retreat of approximately 2 to 5 m per year in some marsh wetlands (Day et al., 2023; Yao et al., 2022); the Nile Delta exhibited coexistence of erosion and sedimentation from 1984 to 2018, with eroded coastlines comprising 44.2%, accreted coastlines 45%, and stable coastlines 10.8% (Abou Samra and Ali, 2021). At the same time, the coastline of YRD is also undergoing significant changes (Wang, 2022).

The YRD coastal zone exhibits a mutual constraint mechanism among the three elements of matter, energy, and space. When the balance of matter and energy is disrupted, the process of establishing a new equilibrium is manifested as the spatial advancement or retreat of the interaction region between these elements. The boundary changes between the old and new interaction regions are reflected as coastline changes on a planar surface (Gao et al., 2023; 2024). The modern YRD was formed after the Yellow River breached its levees at Tongwaxiang in Lanyang, Henan, in June 1855, diverting its course to Tiemenguan in Lijin County (Gao et al., 2018; Liu et al., 2018). This delta, shaped by the sediment load carried by the Yellow River, is continually elevated and expanded by natural forces such as waves and tides, resulting in extensive mudflat landscapes. It is one of the world's most intact and youngest wetland ecosystems in the warm temperate zone. It serves as a major area for oil resources, coastal saltworks, and fisheries development in China. The YRD holds significant

importance in global wetland ecosystem research and has substantial economic value (Zhu et al., 2024; Sun et al., 2024). However, the extensive development of the delta, land subsidence, rising relative sea levels, and intensified human activities have altered the environmental and ecological balance of the YRD (Wu et al., 2023; Wang et al., 2020). These changes have significantly reduced biodiversity (Fu, 2020), consequently affecting the cycle, accumulation, and storage of carbon within the wetland ecosystems (Maier et al., 2021). In 2020, with the proposal of the dual-carbon strategy, studying coastline changes in the YRD became crucial for understanding delta evolution in the context of human activities. This research provides scientific guidance for the comprehensive management, erosion prevention, and future high-quality development of the YRD (Liu, 2022).

The terminal course of the Yellow River has undergone frequent diversions, resulting in over 50 breaches to date, with ten major diversions forming ten sediment lobes. Consequently, the evolution of the coastline has been highly complex (Liu, 2017). Decades of water and sediment regulation and development activities have led to frequent changes in the coastal environments across different regions of the YRD, fostering the development of sub-depositional environments. These processes have resulted in distinct patterns of coastline changes, with increasingly differentiated mechanisms of influence (Zuo et al., 2024; Ren, 2023). In recent years, many studies on the YRD's coastline have focused on the extraction of the overall coastline and the analysis of basic shoreline change characteristics (Ma, 2008; Wang, 2022), primarily addressing the overall coastline changes within the study area. However, there has been a lack of analysis focused on coastline evolution under specific environmental changes (Zhang, 2021). Additionally, studies on the factors influencing coastline changes typically emphasize the impact of human activities, with little to no mention of the role of natural factors (Chu et al., 2020). The modern coastline of the YRD is predominantly artificial, with silty mud and fine sand beaches supplementing it. In this study, the coastline is defined as the boundary between land and water, with an emphasis on interpreting artificial coastlines (Li K. et al., 2023). Therefore, this study integrates the strengths of various coastline analysis methods to examine the unique evolutionary processes of the modern YRD, summarizing its coastline evolution patterns and identifying key factors and mechanisms driving these changes. Through this approach, we analyze the delta's responses to Yellow River course shifts and human activities, providing insight into the relationships between natural factors—such as sea level rise, land subsidence, and extreme weather—and coastline changes against the backdrop of global climate change. Emphasis is placed on elucidating how the evolution of different natural environments affects changes in coastlines.

## 2 Materials and methods

### 2.1 Overview of study area

The modern YRD is located in the southern part of Bohai Bay, on the western side of Laizhou Bay, situated between 36°55' and 38°

16°N, and 117°31' and 119°18'E (Liu et al., 2020). Over nearly 170 years of development, the modern YRD fan-shaped alluvial body with Ninghai as the apex, northwest orientation to the estuary of the Tiao River, southwest extension to the estuary of the Xiaoqing River, and eastward extension into the sea has been formed. Due to natural or human factors, the Yellow River channel frequently sways in the modern delta, with a total of about 50 changes in course. Among them, there are three important changes in course, namely: the Shenxiangou River channel in 1954, the Diaokou River channel in 1964, and the Qingshuigou River channel in 1976. The frequent oscillation of the Yellow River channel has greatly changed the hydrodynamic conditions in the coastal area of the YRD, forming a complex sedimentary environment and sedimentary characteristics (Zheng et al., 2015; Meng et al., 2012).

In this study, the coastline of the YRD stretches from Huanghua Port in Cangzhou City, Hebei Province, in the north to the Guangli River estuary in Dongying City, Shandong Province, in the south, located between 37°20' and 38°31'32.10"N, and 117°45' and 119°22'8.45"E (Figure 1). The artificial coastline within the study area primarily consists of the boundaries of aquaculture ponds and coastal dikes, while the natural coastline is predominantly silty and muddy (Wang et al., 2017). From 1984 to 2024, the YRD region has experienced extensive artificial development, land reclamation, port construction, as well as natural erosion and sedimentation, resulting in significant coastline changes (Liu, 2017; Fan, 2019; Chen et al., 2004; Fu Y. T. et al., 2021; Xing et al., 2016).

## 2.2 Data composition and sources

This study collected remote sensing imagery of the YRD from 1984 to 2022. The remote sensing images for 2023 and 2024 were obtained using the GEE remote sensing cloud platform (Table 1). All of the images are Landsat reflectance data. All data were pre-processed and used for subsequent coastline extraction and DSAS analysis (Supplementary Table 1). The measured data of the coastline comes from on-site RTK testing and UAV photography.

## 2.3 Research method

With advancements in remote sensing technology, the use of satellite imagery for coastline interpretation has become a primary method for conducting spatiotemporal analysis and studying coastal stability (Sun et al., 2023; Zhou et al., 2023). Among these, extracting shorelines to analyze coastal change characteristics has become an essential foundational task (Liu and Jezek, 2004; Alesheikh et al., 2007; Chu et al., 2005). Previous studies have widely applied methods such as the Digital Shoreline Analysis System (DSAS) (Ma et al., 2022), object-oriented classification (Wu et al., 2018), improved normalized water index (Kim et al., 2013), box-counting method (Xu J. et al., 2014), GIS systems (Duan et al., 2021), and enhanced coastline generation algorithms (Xia et al., 2021) to analyze coastline evolution across different regions

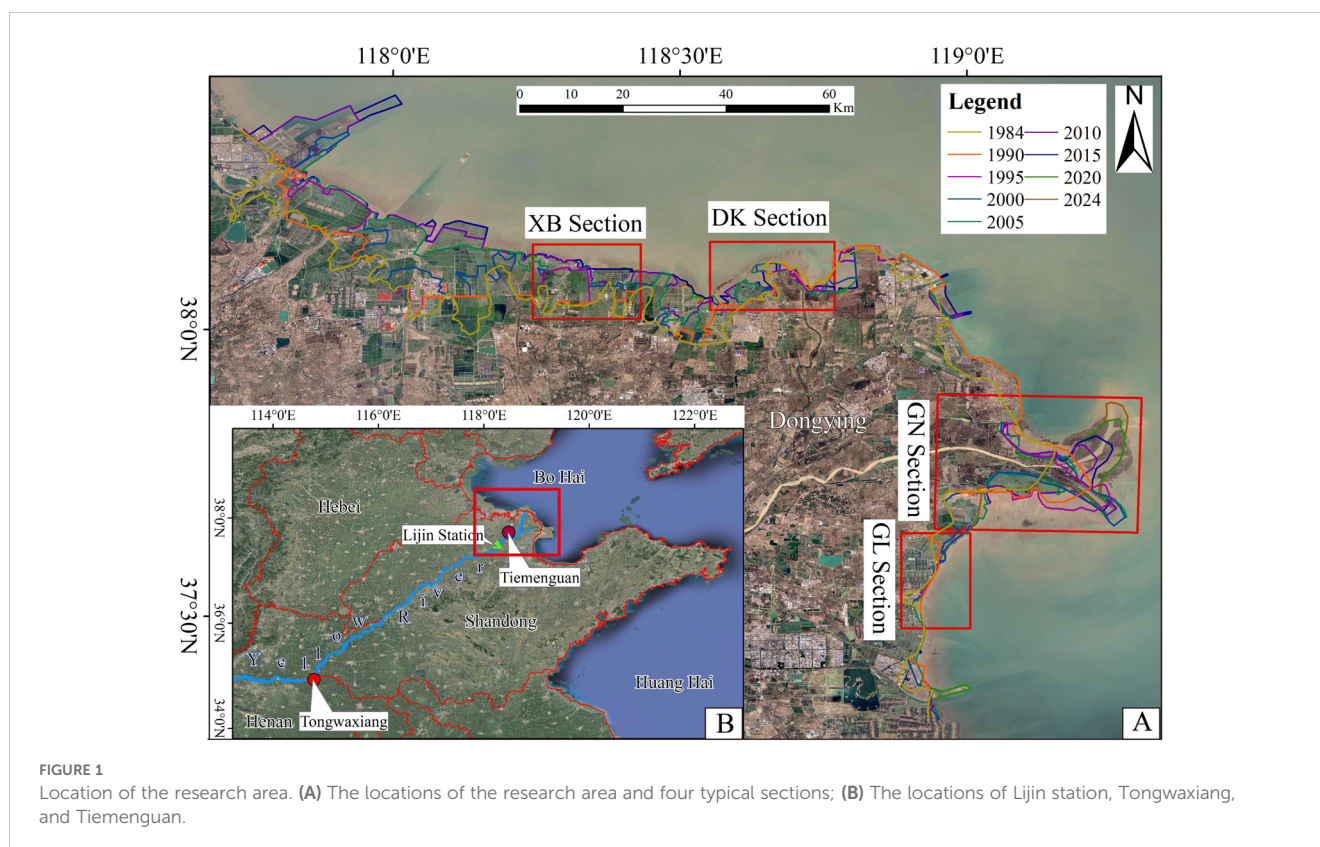


TABLE 1 Research method and selected years.

Method	Years
Shoreline Interpretation	1984, 1986, 1988, 1990, 1994, 1995, 1997, 2000, 2003, 2005, 2008, 2010, 2013, 2015, 2020, 2022, 2023, 2024
GEE	2023, 2024
DSAS Model	1984, 1990, 1995, 1997, 2000, 2005, 2010, 2015, 2020, 2022, 2024

and time scales. Among these methods, the DSAS is currently the most commonly used and efficient system for analyzing the rates of spatiotemporal changes in coastlines (Shen et al., 2020). DSAS enables quantitative analysis of coastline changes using interpreted data from different periods and can work in conjunction with other engineering projects. It has been widely employed both domestically and internationally (Li et al., 2022), playing a significant role in various areas such as coastline migration (Nassar et al., 2019), coastal erosion (Dong et al., 2023), impacts of coastal engineering protection (Paul et al., 2022), and coastal ecosystem changes (Thakur et al., 2021). Therefore, we chose to use the DSAS model to complete this study.

This study employs a detailed approach to analyze the overall coastline changes in the YRD. Based on various coastal environments, four typical sections were selected from north to south: Yangkejun Ditch Section (XB Section, newly constructed dam section), Diaokou River Estuary Section (DK section, eroding section), Qingshuigou Section (GN Section, accumulating section), and Guangli River Estuary Section (GL Section, stable section). Visual interpretation was used to extract the coastline in YRD from 1984 to 2024, and it was combined with the Google Earth Engine (GEE) remote sensing cloud computing platform for cross-validation in some areas of the GN section. RTK (Real-Time Kinematic) and DJI Phantom 4 drones were employed to survey the coastline of typical and complex sections, with specific landmarks extracted to improve interpretation accuracy. The DSAS model was then used to analyze the characteristics of coastline changes and the factors influencing these changes in four typical sections of the YRD (Figure 2).

### 2.3.1 Coastline interpretation and coastline changes

#### 2.3.1.1 Visual Interpretation and Extraction of Coastlines

The collected remote sensing images were visually interpreted to extract coastlines, categorizing them into artificial and natural coastlines. After cloud removal processing using the GEE platform, the Automated Water Extraction Index (AWEI) was calculated. The Otsu method (OTSU) was employed for binary threshold segmentation to determine the optimal threshold for water pixels. The GEE platform’s built-in algorithm was then used to remove inland water bodies and small islands. Finally, the data was converted from raster to vector to obtain the coastline data.

(i) Automated Water Extraction Index (AWEI): AWEI enhances the accuracy of water body extraction amidst various environmental noises while providing a stable threshold. The formula is as follows:

$$AWEI=4 \times (GREEN-SWIR1)-(0.25 \times NIR+2.75 \times SWIR2)$$

Where GREEN represents the green band of the selected remote sensing image, NIR represents the near-infrared band, and SWIR1 and SWIR2 represent the shortwave infrared bands 1 and 2, respectively.

(ii) OTSU: Also known as the maximum between-class variance method, OTSU is an algorithm for determining thresholds, first proposed by scholar Nobuyuki Otsu in 1979. This method is commonly used for adaptive calculation in image binarization. The existing OTSU code in the GEE platform can be directly invoked for computation (Donchyts et al., 2016).

#### 2.3.1.2 Moving average analysis and polynomial fitting of coastline length

The total length of the YRD’s coastlines over the years was analyzed using the moving average method. The lengths and proportions of artificial and natural coastlines were analyzed using polynomial fitting.

(i) Moving Average Method: This method eliminates irregular fluctuations and other variations in a time series through moving averages, revealing the long-term trend of the series. Depending on the weights assigned to each element in the forecast, it can be



FIGURE 2 UAV images. (A) XB section (Yangkejun Ditch); (B) GN section (Qingshuigou).

classified as a simple moving average or a weighted moving average. This study employs the simple moving average with the formula:

$$Y_{t+1} = F_t = (A_t + A_{t-1} + A_{t-2} + \dots + A_{t-n+1}) / n$$

Where  $Y_{t+1}$  represents the forecast value for the next period,  $A_{t-1}$  represents the actual value of the previous period,  $n$  represents the number of periods ( $t > n \geq 2$ ), and  $A_{t-n+1}$  represents the actual values of the previous  $n-1$  periods.

(ii) Intensity of Coastline Changes: This method is used to measure the difference in the rate of change of coastline length over time, in order to explore the spatiotemporal characteristics of different types of coastlines in the research area. The Specific formula is as follows:

$$LCI_{ij} = \frac{L_i - L_j}{L_j \times (i - j)}$$

Where  $LCI_{ij}$  represents the intensity of coastline changes from the year  $i$  to  $j$ .  $L_i$  and  $L_j$  represent the length of the coastline in the  $i$ -th and  $j$ -th year, respectively.  $LCI_{ij}$  has both positive and negative values. A positive  $LCI_{ij}$  indicates an increase in coastline length, while a negative  $LCI_{ij}$  indicates a decrease in coastline length. The larger the absolute value of  $LCI_{ij}$ , the greater the change in coastline length.

(iii) Polynomial Fitting: This study uses a traditional second-order polynomial for fitting, with the formula:

$$y = ax^2 + bx + c$$

### 2.3.2 Analysis of coastline changes based on DSAS

The DSAS, developed by the United States Geological Survey (USGS), is used to analyze coastline movement and change rates based on the ArcGIS 10.8 platform. The operation of DSAS involves six steps: (1) Extraction and integration of coastlines; (2) Drawing baselines and setting DSAS baseline param; (3) Setting coastline param and generating the direction of transects; (4) Calculating the distance between baselines and coastlines; (5) Automatically calculating coastline change rates using different models, such as the End Point Rate (EPR) and Net Coastline Movement (NSM); (6) Adjusting baselines, repeating steps (2) to (5), and optimizing the results. This study primarily uses the EPR model to calculate coastline change rates.

The EPR model is primarily used to monitor and calculate coastline changes. It calculates the change rate based on the distance between coastlines at different times along the transects and the corresponding time intervals. The formula is as follows:

$$EPR_{m(i,j)} = \frac{D_{mj} - D_{mi}}{T}$$

Where  $EPR_{m(i,j)}$  represents the change rate of the coastline at times  $i$  and  $j$  along the  $m$ th baseline,  $D_{mi}$  and  $D_{mj}$  represent the distances from the intersections of the coastlines at times  $i$  and  $j$  to the baseline along the  $m$ th transect, respectively, and  $T$  is the time interval between times  $i$  and  $j$ . The change rate is expressed in negative or positive values of m/a, where negative values indicate

erosion, positive values indicate accretion, and zero indicates no change in coastline position. The erosion, stable, and accreting coastline standards are set as  $EPR \leq -0.5$  m/a,  $-0.5$  m/a <  $EPR < 0.5$  m/a, and  $EPR \geq 0.5$  m/a, respectively.

The NSM model detects coastline movement, representing the net distance between two coastlines.

## 3 Results

### 3.1 Overall changes in the coastline

The interpreted region has an average total coastline length of 398.9 km, with the minimum and maximum values recorded in 1988 and 2000 at 357.2 km and 440.7 km, respectively. The period from 1984 to 2000 witnessed a rapid expansion of artificial coastlines, while the growth of these coastlines gradually stabilized after 2000. In contrast, the total length of natural coastlines experienced a general trend of reduction throughout most of the years between 1984 to 2024 (Table 2). Figure 3 represents a 2-period moving average analysis of the total coastline length, with a standard error of within 5%, indicating that the variations in total coastline length are relatively small compared to the total length, maintaining an overall balance. The primary reason for this stability is the alternating evolution between different types of coastlines within the region, where the increase in artificial coastlines compensates for the decrease in natural coastlines. Polynomial fitting results indicate that artificial coastlines have consistently shown a rapid growth trend, with an  $R^2$  of 0.9154, while natural coastlines have exhibited a rapidly decreasing trend, with an  $R^2$  of 0.965 (Figure 3).

### 3.2 Changes in coastline during different periods

#### 3.2.1 Rapid transformation period from 1984 to 2000

From 1984 to 2000, the YRD experienced an overall increase in coastline length, alongside a rapid shift from natural to artificial coastlines. The total coastline length increased from 398.96 km to 440.65 km, while the length of artificial coastlines expanded from 80.19 km to 320.06 km, raising its proportion from 20.1% to 72.63%. Meanwhile, natural coastlines decreased from 318.77 km to 120.60 km, with their proportion declining from 79.9% to 27.37%. Two significant time points stand out during this period: (i) Between 1986 and 1988, the proportion of artificial coastlines surpassed that of natural coastlines for the first time. The share of natural coastlines dropped from 69.35% in 1986 to 45.18% in 1988, while the share of artificial coastlines rose from 30.65% to 54.82%; (ii) The period from 1997 to 2000 witnessed the fastest growth of artificial coastlines, expanding by approximately 67 km, with an annual growth rate of 22.3 km/a. During this period, natural coastlines saw their most significant decrease between 1986 and 1988, shrinking by 123.4 km, with an average annual loss exceeding 41.1 km/a (Figure 4).

TABLE 2 The Coastline Length, Proportion of YRD from 1984 to 2024.

Years	Length and Proportion						Total Length Km	Moving Average Km	Intensity of Total Coastline Changes %
	Artificial Coastline Km	Proportion of AC %	Intensity of AC Changes %	Natural Coastline Km	Proportion of NC %	Intensity of NC Changes %			
1984	80.19	20.10%	-	318.77	79.90%	-	398.96	-	-
1986	125.88	30.65%	28.49%	284.8	69.35%	-5.33%	410.70	404.83	1.47%
1988	195.84	54.82%	27.78%	161.39	45.18%	-21.67%	357.22	383.96	-6.51%
1990	200.56	53.99%	1.21%	170.88	46.01%	2.94%	371.44	364.33	1.99%
1994	233.37	60.05%	4.09%	155.23	39.95%	-2.29%	388.60	380.02	1.15%
1995	239.84	60.77%	2.77%	154.81	39.23%	-0.27%	394.65	391.62	1.56%
1997	253.06	60.33%	2.75%	166.43	39.67%	3.75%	419.49	407.07	3.15%
2000	320.06	72.63%	8.83%	120.60	27.37%	-9.18%	440.65	430.07	1.68%
2003	328.37	81.18%	0.87%	76.13	18.82%	-12.29%	404.50	422.58	-2.73%
2005	334.51	84.59%	0.93%	60.96	15.41%	-9.96%	395.47	399.98	-1.12%
2008	324.95	85.54%	-0.95%	54.95	14.46%	-3.29%	379.90	387.68	-1.31%
2010	322.47	82.60%	-0.38%	67.93	17.40%	11.81%	390.40	385.15	1.38%
2013	332.49	91.02%	1.04%	32.80	8.98%	-17.24%	365.29	377.84	-2.14%
2015	361.95	91.51%	4.43%	33.58	8.49%	1.18%	395.53	380.41	4.14%
2020	356.52	86.56%	-0.30%	55.38	13.44%	12.98%	411.89	403.71	0.83%
2022	358.08	85.56%	0.22%	60.44	14.44%	4.57%	418.51	415.20	0.80%
2024	364.23	86.78%	0.86%	55.49	13.22%	-4.09%	419.72	419.12	0.14%

### 3.2.2 Slow transition period from 2000 to 2015

Between 2000 and 2015, the total coastline length gradually declined, and the coastline transformation rate slowed. From 2000 to 2005, the coastline continued to contract, following the transformation trend from the previous phase, with the

proportion of artificial coastlines increasing further from 72.63% to 84.59%. Between 2005 and 2010, the total coastline length changed by less than 5 km, and the proportion of artificial coastlines slightly decreased to 82.60%. From 2010 to 2015, the total coastline length increased again, although the proportion of

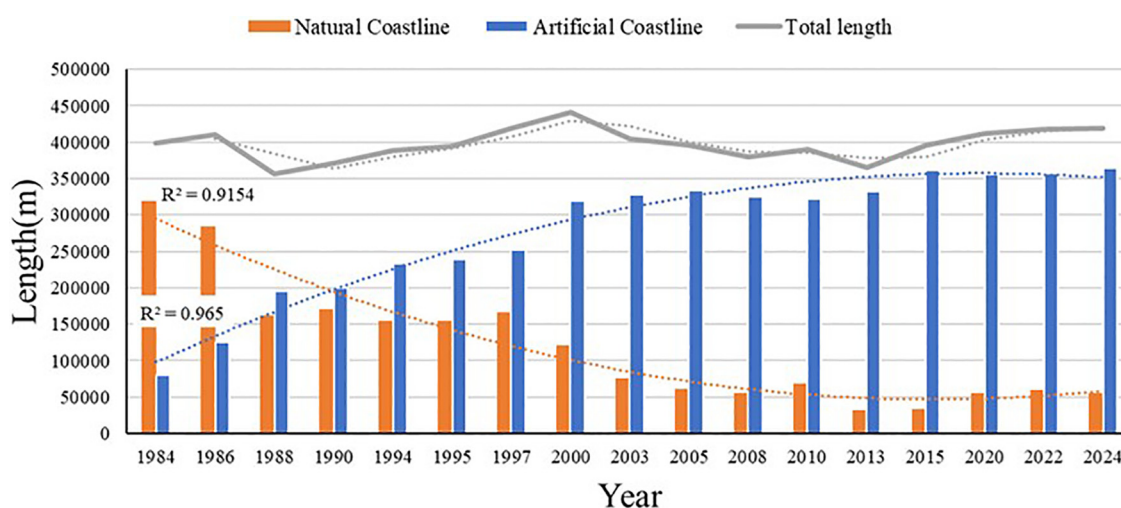
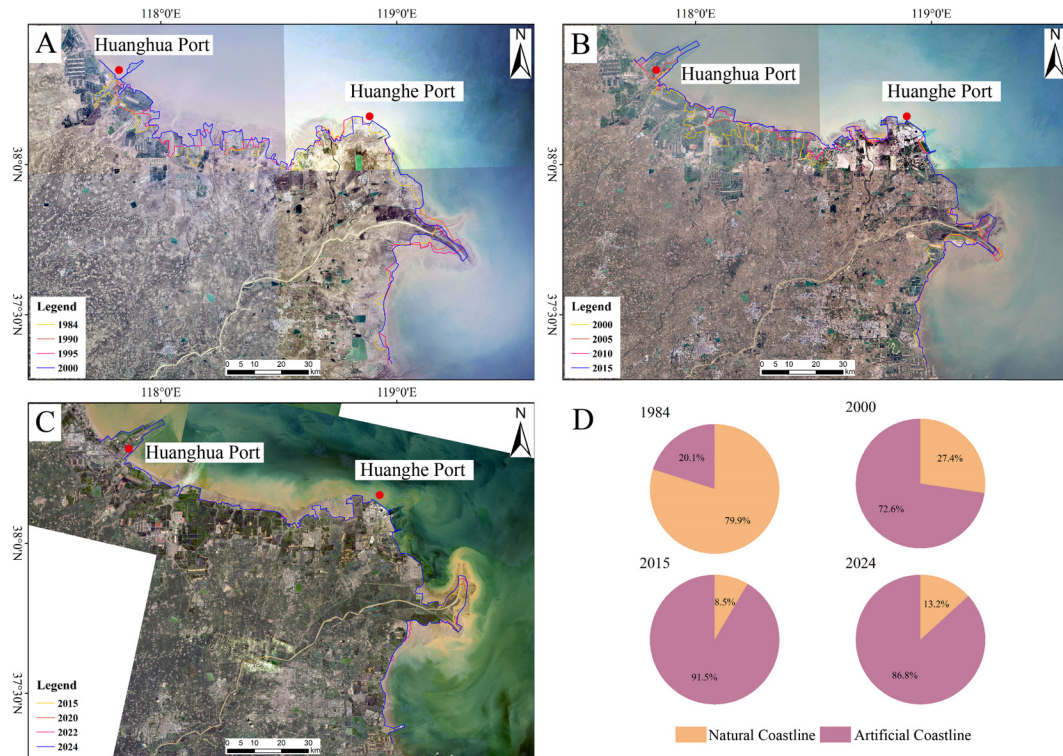


FIGURE 3 Changes in the coastline of the YRD from 1984 to 2024.



**FIGURE 4** Changes in coastline types: (A) 1984-2000; (B) 2000-2015; (C) 2015-2024; (D) The proportion of natural coastline and artificial coastline in different years.

natural coastlines continued to decline. By 2015, the proportion of artificial coastlines exceeded 90% for the first time, reaching the highest percentage in the past 40 years, while the natural coastline length remained relatively stable, though its share further decreased (Figure 4).

### 3.2.3 Stabilization period from 2015 to 2024

From 2015 to 2024, the total coastline length showed an upward trend, stabilizing the transformation rate. The annual rate of change remained steady at approximately 3 km/a. During this period, artificial coastlines reached a relatively stable state, consistently accounting for about 85% of the total coast. The proportion of natural coastlines slightly increased, rising from 8.49% to 13.22% (Figure 4).

## 3.3 Results of typical coastline changes

### 3.3.1 XB section (Yangkejun Ditch) coastline changes

From 1984 to 2024, the XB section exhibited continuous accretion, with an average accretion rate of 186.97 m/a, a maximum accretion rate of 281.19 m/a, and the furthest coastline advancement reaching 11,247.52 m (Figure 5D and Supplementary Table 2D).

#### 3.3.1.1 Rapid transition phase from 1984 to 2000

Between 1984 and 2000, the XB section coastline generally advanced seaward, with 91.41% of the section experiencing accretion at an average rate of 302.76 m/a. In contrast, 3.68% of the section underwent erosion at an average rate of 32.02 m/a, while 4.91% remained stable. The EPR ranged from a maximum of 524.26 m/a to a minimum of -52.22 m/a. The NSM values ranged from 8388.12 m to -835.59 m. The average coastline change rate was 275.58 m/a, with a net coastline movement of 4,409.23 m. During this period, areas A1 and A3 were significantly impacted by the expansion of coastal aquaculture, with average coastline change rates of 321.74 m/a and 204.31 m/a, respectively. Erosion in area A2 was attributed to the artificial straightening of the original sinuous natural coastline, with an average coastline change rate of -32.03 m/a (Figure 5A and Supplementary Table 2A).

#### 3.3.1.2 Slow transition phase from 2000 to 2015

From 2000 to 2015, the XB section continued to experience accretion, with 98.79% of the section showing an average accretion rate of 210.31 m/a. Only 1.22% of the section underwent erosion at an average rate of 0.95 m/a. The EPR values ranged from a maximum of 668.57 m/a to a minimum of -1.29 m/a. The NSM values ranged from 10,026.77 m to -19.35 m. The average coastline change rate was 207.73 m/a, with a net coastline movement of 3,115.40 m. In this period, the coastline of the XB section advanced

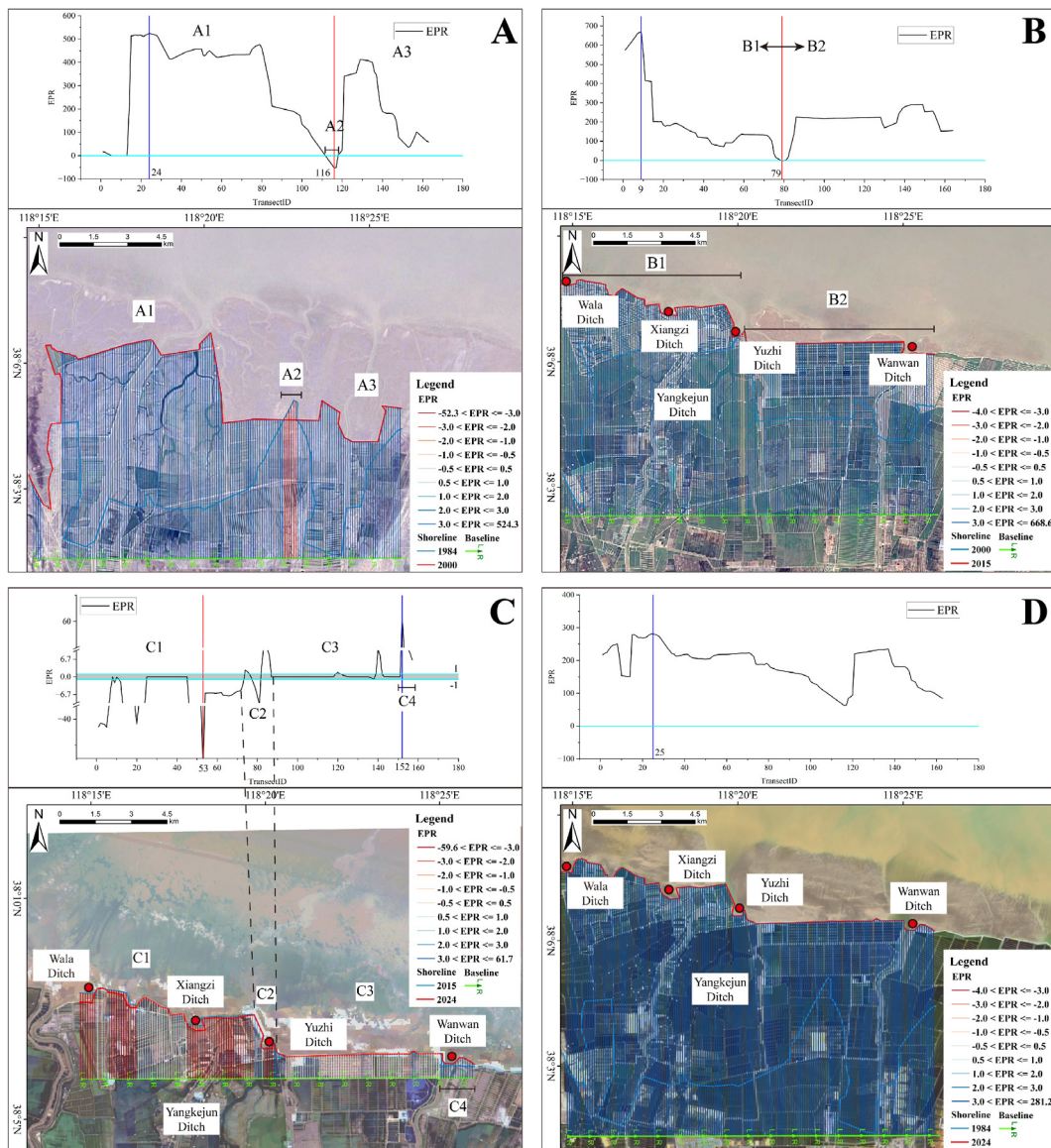


**FIGURE 5**  
XB section coastline changes. **(A)** Rapid transition phase from 1984 to 2000; **(B)** Slow transition phase from 2000 to 2015; **(C)** Stable phase from 2015 to 2024; **(D)** Overview of XB section (Yangkejun Ditch) coastline changes from 1984 to 2024. The color lines of the vertical baseline are interpolated lines generated by the DSAS model, shown as EPR results in the figure.

rapidly seaward for a decade, with areas B1 and B2 predominantly accreting (Figure 5B and Supplementary Table 2B).

### 3.3.1.3 Stable phase from 2015 to 2024

Between 2015 and 2024, the artificial coastline of the XB section remained largely stable, with the natural coastline experiencing slight erosion. Accretion occurred in 18.18% of the section at an average rate of 15.89 m/a, while erosion affected 33.94% of the section at an average rate of 14.70 m/a. Stable sections accounted for 47.88%. The EPR values ranged from a maximum of 61.7 m/a to a minimum of -59.59 m/a. The NSM values ranged from 555.43 m to -68.1 m. The average coastline change rate was -2.28 m/a, with a net coastline movement of -20.55 m. In areas C1 and C2, however, some natural coastlines at river mouths like Yuzhigou, Xiangzigou,

and Wala Gou experienced slight erosion, with average coastline change rates of -10.9 m/a and 3.19 m/a, respectively. Area C3 remained stable overall, while area C4 experienced minor accretion at the bay bayou, with an average coastline change rate of 24.95 m/a (Figure 5C and Supplementary Table 2C).

### 3.3.2 DK section (Diaokou River Estuary) coastline changes

From 1984 to 2024, the DK section exhibited both accretion and erosion, with 52.25% of the section experiencing accretion at an average rate of 49.71 m/a and 47.75% experiencing erosion at an average rate of 23.88 m/a. The EPR values ranged from 94.58 m/a to a minimum of -81.98 m/a. The NSM values ranged from 3,783.5 m to -3,279.07 m. Significant differences in erosion and accretion were

observed across the Diaokou Yellow River Old Course. The western side saw the coastline pushed outward due to the construction of aquaculture ponds and other artificial structures, while the eastern Feiyan Beach area experienced overall erosion, with some parts remaining stable or advancing slightly (Figure 6D and Supplementary Table 3D).

### 3.3.2.1 Rapid transition phase from 1984 to 2000

From 1984 to 2000, the DK section primarily experienced erosion, with 21.79% of the section undergoing accretion at an average rate of 60.24 m/a, 65.36% undergoing erosion at an

average rate of 48.14 m/a, and 12.85% remaining stable. The EPR values ranged from a maximum of 118.95 m/a to a minimum of -133.58 m/a. The NSM values ranged from 1,903.22 m to -2,137.35 m. The average coastline change rate was -18.34 m/a, with a net coastline movement of -293.53 m. During this period, following the alteration of the Yellow River's flow in 1976, the disruption of sediment transport led to a significant change in hydrodynamic conditions in area D3, specifically at Feiyan Beach, rendering it a primary erosion zone during this period, with an average coastline change rate of -63.44 m/a (Figure 6A and Supplementary Table 3A).

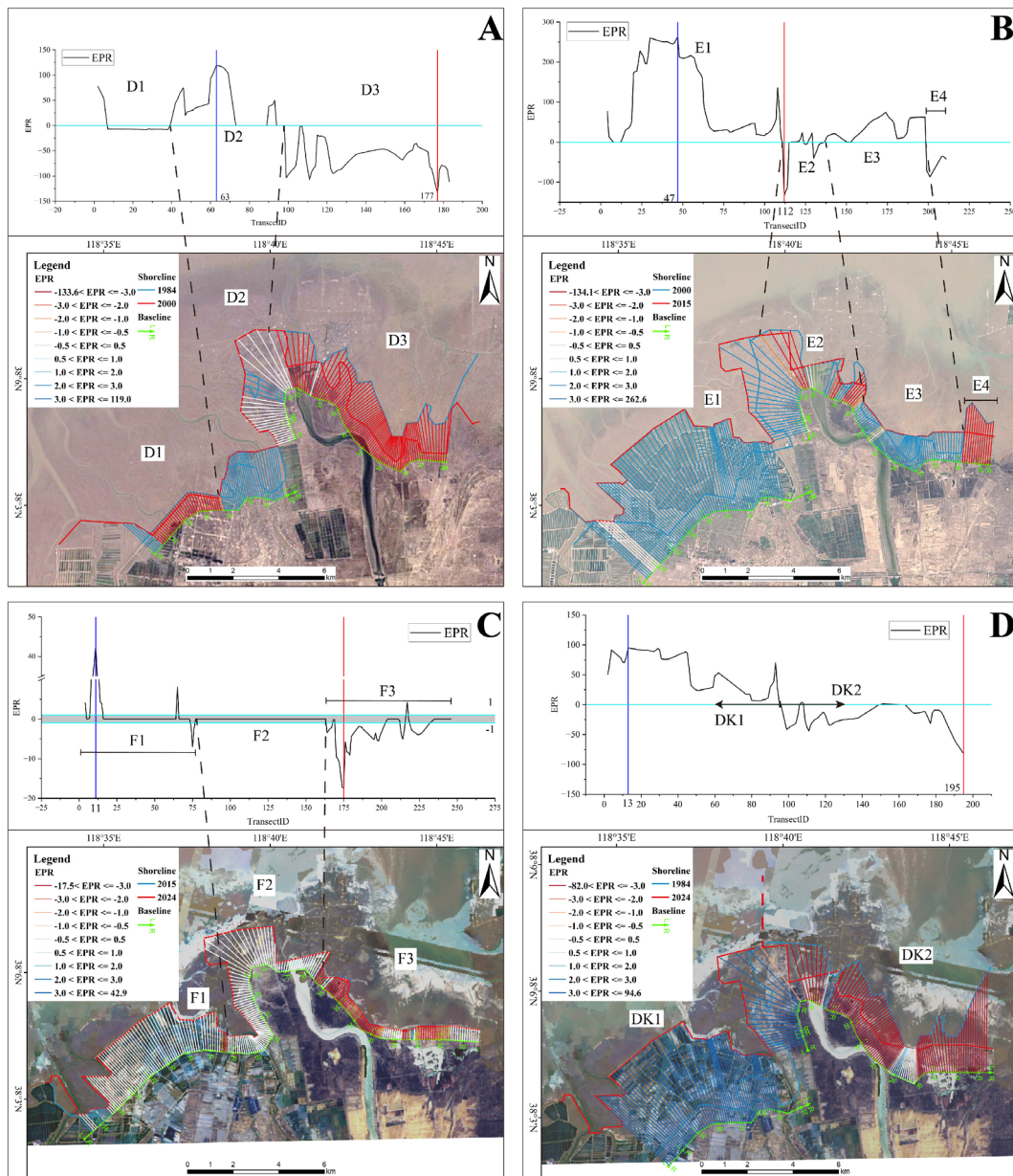


**FIGURE 6** DK section coastline changes. (A) Rapid transition phase from 1984 to 2000; (B) Slow transition phase from 2000 to 2015; (C) Stable phase from 2015 to 2024; (D) Overview of DK section (Diaokou River Estuary) coastline changes from 1984 to 2024. The color lines of the vertical baseline are interpolated lines generated by the DSAS model, shown as EPR results in the figure.

### 3.3.2.2 Slow transition phase from 2000 to 2015

From 2000 to 2015, the DK section primarily exhibited accretion, with 82.14% of the section undergoing accretion at an average rate of 83.81 m/a, 13.78% undergoing erosion at an average rate of 46.10 m/a, and 4.08% remaining stable. The EPR values ranged from a maximum of 262.51 m/a to a minimum of -134.1 m/a. The NSM values ranged from 3,936.94 m to -2,011.1 m. The average coastline change rate was 62.49 m/a, with a net coastline movement of 937.12 m. In this period, noticeable accretion occurred along the western part of the coastline in area E1, with an average coastline change rate of 118.29 m/a. Areas E2 to E4 continued to exhibit coastline retreat due to the regulation of artificial coastlines, particularly in area E4, which demonstrated an average coastline change rate of -58.39 m/a (Figure 6B and Supplementary Table 3B).

### 3.3.2.3 Stable phase from 2015 to 2024

From 2015 to 2024, the DK coastline primarily stabilized, with 4.94% of the section undergoing accretion at an average rate of 15.70 m/a, 24.28% undergoing erosion at an average rate of 4.49 m/a, and 70.78% remaining stable. The EPR values ranged from a maximum of 42.82 m/a to a minimum of -17.46 m/a. The NSM values ranged from 385.51 m to -157.22 m. The average coastline change rate was -0.32 m/a, with a net coastline movement of -2.88 m. Post-2015, with the construction of river mouth dams, the coastlines of areas F1 and F2 stabilized, while area F3, encompassing Feiyan Beach, remained largely stable, exhibiting only minor erosion in select regions, with an average coastline change rate of -3.01 m/a (Figure 6C and Supplementary Table 3C).

## 3.3.3 GN section (Qingshuigou) coastline changes

Between 1997 and 2024, the GN section coastline primarily experienced erosion. Accretion was observed in 38.02% of the coastline, with an average accretion rate of 151.95 m/a, while erosion affected 53.33% of the coastline, with an average erosion rate of 62.75 m/a. Stability was maintained in 8.64% of the coastline. The EPR values ranged from a maximum of 577.74 m/a to a minimum of -170.16 m/a. The NSM values ranged from 15,599.03 m to -4,594.27 m. Distinct zones of accretion and erosion were evident, with the old Qingshuigou estuary acting as the boundary. To the north, the coastline exhibited overall accretion, particularly around the Qingshuigou No. 8 distributary (Q8) estuary that was redirected in 1996. To the south, the old estuary and its surroundings experienced erosion, primarily due to the transformation of the natural coastline into an artificial one for ecological protection, resulting in significant retreat (Figure 7E and Supplementary Table 4E).

### 3.3.3.1 First rapid transition phase from 1984 to 1997

From 1984 to 1997, the GN section coastline primarily experienced accretion, with 48.87% of the section undergoing accretion at an average rate of 222.82 m/a, 32.75% undergoing erosion at an average rate of 127.21 m/a, and 18.39% remaining stable. The EPR values ranged from a maximum of 1,158.71 m/a to

a minimum of -233.00 m/a. The NSM values ranged from 15,060.02 m to -3,028.37 m. The average coastline change rate was 67.22 m/a, with a net coastline movement of 873.74 m. In this period, it predominantly experienced accretion, particularly in area G1, due to the construction of the Gulong Oilfield, leading to continuous accretion of surrounding coastlines. In area G2, the conversion of the natural coastline to an artificial one resulted in some coastline retreat, with an average coastline change rate of -161.11 m/a. Simultaneously, during this period, the ongoing sediment delivery from the Yellow River led to significant accretion in the coastal area of G3, with an average coastline change rate of 474.34 m/a (Figure 7A and Supplementary Table 4A).

### 3.3.3.2 Second rapid transition phase from 1997 to 2005

From 1997 to 2005, the GN section coastline primarily experienced erosion, with 25.27% of the section undergoing accretion at an average rate of 350.36 m/a, 65.12% undergoing erosion at an average rate of 259.30 m/a, and 9.61% remaining stable. The EPR values ranged from a maximum of 847.45 m/a to a minimum of -614.69 m/a. The NSM values ranged from 6,779.59 m to -4,917.53 m. The average coastline change rate was -80.31 m/a, with a net coastline movement of -642.44 m. In this period, following the alteration of the Yellow River's course in 1996, an accretion area emerged in the northern part of area H5, with an average coastline change rate of 68.41 m/a. Areas H6 and H8, on both sides of the former Yellow River mouth, experienced coastline retreat due to the construction of artificial coastlines within the YRD Ecological Protection Area, with average coastline change rates of -94.80 m/a and -394.35 m/a, respectively (Figure 7B and Supplementary Table 4B).

### 3.3.3.3 Slow transition phase from 2005 to 2015

From 2005 to 2015, the GN section coastline primarily experienced accretion, with 61.69% of the section undergoing accretion at an average rate of 215.95 m/a, 14.67% undergoing erosion at an average rate of 52.09 m/a, and 23.55% remaining stable. The EPR values ranged from a maximum of 840.14 m/a to a minimum of -351.26 m/a. The NSM values ranged from 8,401.38 m to -3,512.61 m. The average coastline change rate was 125.53 m/a, with a net coastline movement of 1,255.32 m. During a period of rapid coastline advancement, the northern part of the Gulong Oilfield area remained stable, while the new river mouth at Qingshuigou advanced westward due to sediment transport from the Yellow River, with an average coastline change rate of 390.75 m/a. The cessation of sediment transport in the former river mouth region altered local hydrodynamic conditions, leading to some retreat in area I5, with an average coastline change rate of -114.47 m/a (Figure 7C and Supplementary Table 4C).

### 3.3.3.4 Stable phase from 2015 to 2024

From 2015 to 2024, the GN section coastline exhibited stable accretion, with 28.65% of the section undergoing accretion at an average rate of 160.02 m/a, 23.59% undergoing erosion at an average rate of 72.84 m/a, and 47.76% remaining stable. The EPR values ranged from a maximum of 811.87 m/a to a minimum of

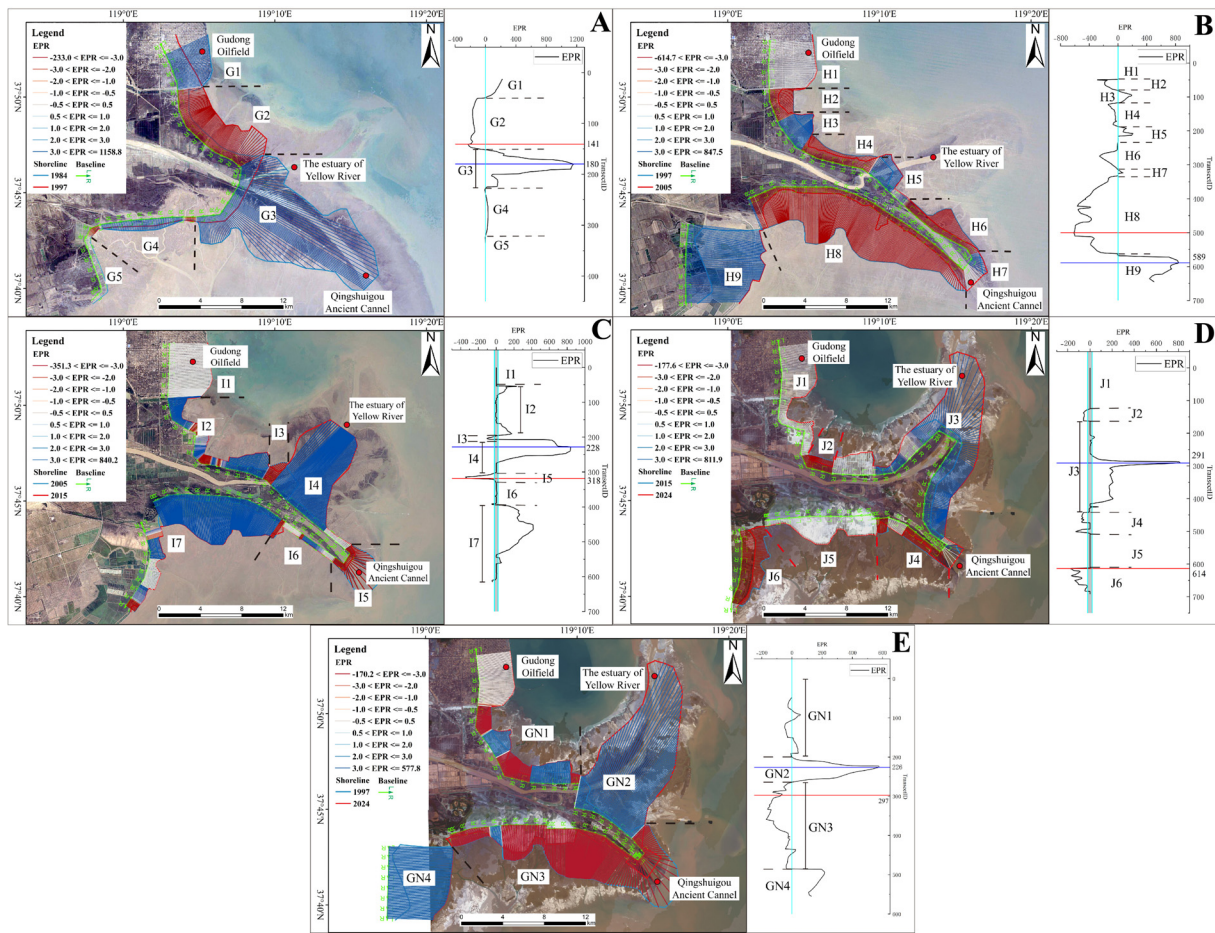


**FIGURE 7** GN section coastline changes. (A, B) Rapid transition phase from 1984–2005; (C) Slow transition phase from 2005 to 2015; (D) Stable phase from 2015 to 2024; (E) Overview of GN section (Qingshuigou) coastline changes from 1984 to 2024. The color lines of the vertical baseline are interpolated lines generated by the DSAS model, shown as EPR results in the figure.

-177.55 m/a. The NSM values ranged from 7,309.07 m to -1,598.47 m. The average coastline change rate was 28.67 m/a, with a net coastline movement of 258.12 m. In this period, the GN section remained largely stable, with the artificial coastlines around the Gulong Oilfield remaining consistent. In area J3, the coastline continued to accrete westward due to sediment delivery from the Yellow River, with an average coastline change rate of 118.23 m/a. The former river mouth’s retreat stabilized, while the artificial coastline in area J5’s ecological protection zone remained stable. Coastal retreat occurred in area J6 due to aquaculture regulations, with an average coastline change rate of -86.29 m/a (Figure 7D and Supplementary Table 4D).

### 3.3.4 GL section (Guangli River Estuary) coastline changes

Between 1984 and 2024, the coastline at the GL section primarily advanced seaward due to sediment accretion. Accretion was observed in 69.73% of the coastline, with an average accretion rate of 35.09 m/a, while erosion affected 30.27% of the coastline, with an average erosion rate of 10.77 m/a. The EPR values ranged from a maximum of 90.35 m/a to a minimum of -22.57 m/a. The

NSM values ranged from 3,613.85 m to -902.89 m. Over the 40 years, the coastline changes were primarily driven by the construction of artificial coastlines. The coastline was divided into northern and southern parts by the Yongfeng River. The north part experienced significant accretion, while the central part experienced slight erosion. The southern part experienced significant erosion due to the retreat of the natural coastline following artificial construction (Figure 8D and Supplementary Table 5D).

#### 3.3.4.1 Rapid transition from 1984 to 2000

From 1984 to 2000, the coastline at the GL section primarily experienced accretion, with 70.27% of the section undergoing accretion at an average rate of 91.07 m/a, 25.41% undergoing erosion at an average rate of 6.93 m/a, and 4.32% remaining stable. The EPR values ranged from a maximum of 189.56 m/a to a minimum of -16.62 m/a. The NSM values ranged from 3,032.91 m to -265.95 m. The average coastline change rate was 62.24 m/a, with a net coastline movement of 995.77 m. In this period, natural coastlines in areas K1, K2, and K4 were converted to artificial coastlines due to the establishment of coastal aquaculture. Areas K2 and K4 exhibited coastline retreat, with average change rates of

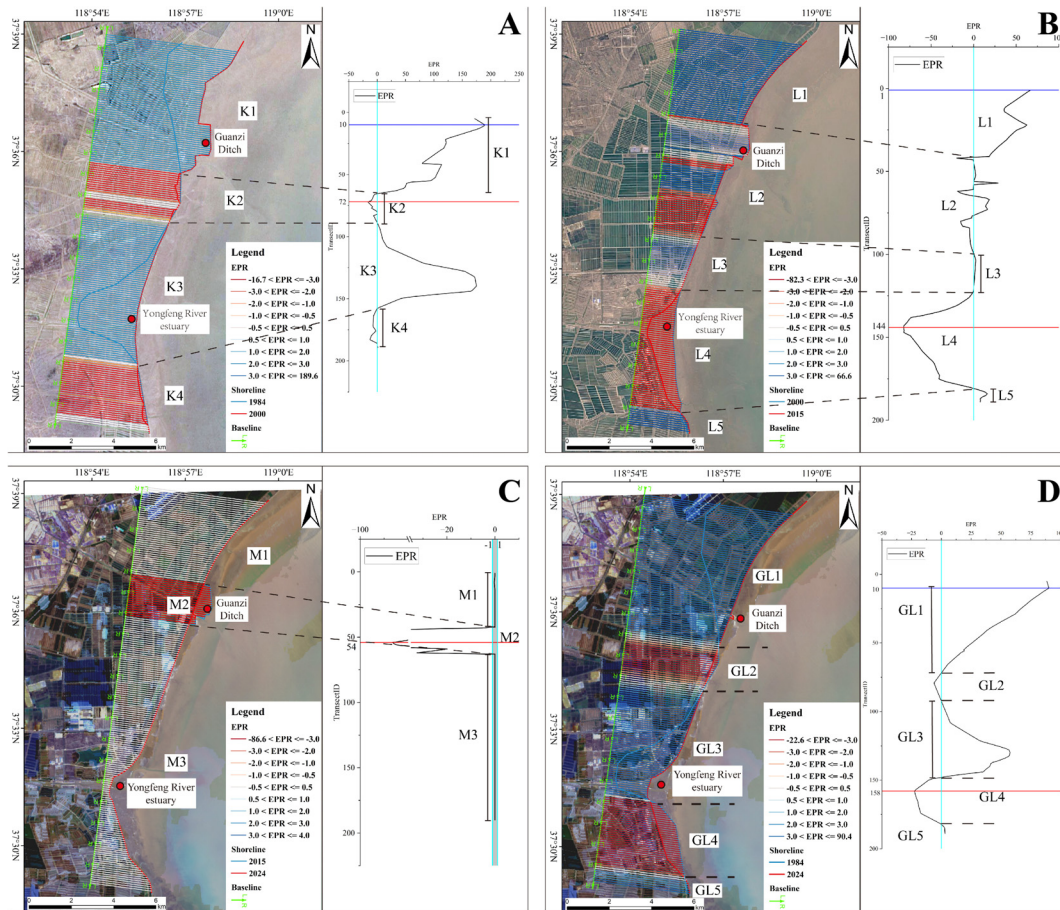


**FIGURE 8** GL section coastline changes. (A) Rapid transition phase from 1984 to 2000; (B) Slow transition phase from 2000 to 2015; (C) Stable phase from 2015 to 2024; (D) Overview of GL section (Guangli River Estuary) coastline changes from 1984 to 2024. The color lines of the vertical baseline are interpolated lines generated by the DSAS model, shown as EPR results in the figure.

-6.75 m/a and -5.66 m/a, respectively. Area K3 experienced coastline expansion seaward following the surrounding artificial coastlines, with an average coastline change rate of 70.73 m/a (Figure 8A and Supplementary Table 5A).

### 3.3.4.2 Slow transition from 2000 to 2015

From 2000 to 2015, the coastline at the GL section primarily experienced accretion, with 47.09% of the section undergoing accretion at an average rate of 23.36 m/a, 44.97% undergoing erosion at an average rate of 35.15 m/a, and 7.94% remaining stable. The EPR values ranged from a maximum of 66.6 m/a to a minimum of -82.22 m/a. The NSM values ranged from 998.75 m to -1,233.01 m. The average coastline change rate was -4.81 m/a, with a net coastline movement of -72.17 m. In this period, the GL section maintained stability with sedimentation; areas L1 and L5 expanded seaward due to the construction of coastal aquaculture ponds, while area L3 remained stable. Minor erosion occurred in the central area L2 due to coastal engineering adjustments. In area L4, the natural coastline at Yongfeng River retreated under the hydrodynamic influence of Laizhou Bay, with an average coastline change rate of -48.2 m/a (Figure 8B and Supplementary Table 5B).

### 3.3.4.3 Stable phase from 2015 to 2024

From 2015 to 2024, the coastline at the GL section stabilized utterly. No accretion was observed, and 10.53% of the coastline experienced erosion at an average rate of 54.24 m/a, while 89.47% remained stable. The EPR values ranged from a maximum of 0 m/a to a minimum of -86.56 m/a. The NSM values ranged from 0 m to -779.28 m. The average coastline change rate was -5.72 m/a, with a net coastline movement of -51.48 m. In this period, the Guangli section remained mostly stable, with area M2's canal experiencing coastline retreat due to the reorganization of abandoned aquaculture ponds, recording an average coastline change rate of -54.24 m/a (Figure 8C and Supplementary Table 5C).

## 4 Discussion

The factors affecting the changes in the coastline of the YRD are mainly divided into natural factors and human factors. Natural factors include the swing of the Yellow River, extreme weather, and the combined effects of sea level rise and land subsidence. Human factors mainly include the development of coastal engineering, such as artificial reclamation and land reclamation.

## 4.1 The impact of swing of the Yellow River

Water and sediment processes have a significant impact on river channel evolution. The processes of water and sediment inevitably lead to river channel evolution. As a critical component of delta systems, river channels provide a direct conduit for delivering terrigenous material, forming the basic framework of deltaic landforms. These channels play a significant role in forming and evolving deltas, transporting nearshore sediments, and coastal erosion in delta regions (Kong et al., 2015). Influenced by natural factors and human activities such as soil and water conservation, construction of hydraulic projects, and water diversion in the Yellow River basin, the water and sediment processes at the Yellow River estuary exhibit significant periodic changes. As a crucial link between the Yellow River basin and marine systems, the river channels at the Yellow River estuary have undergone complex evolutionary responses to adapt to these changes (Chen et al., 2021).

River diversion refers to a river abandoning its original channel to establish a new path due to natural flow breakthroughs or human intervention. Post-diversion, the flow typically completely deviates from the original channel and selects a new route in low-lying areas (Alber and Piégay, 2017). Outlets, specifically in the lower reaches of river estuaries influenced by tidal actions, experience dual forces from runoff and tidal currents. The main flow deviates from the original channel, following new distributaries and outlets to the sea, resulting in the silting and abandonment of the former main channel. This process can also occur through artificial diversion following the excavation of new channels. River distributary channels primarily impact natural coastal regions, with effects most pronounced at river estuaries. The substantial influx of water and sediment from the main river channel forms a rapidly accreting area at the new estuary, altering the erosion and deposition dynamics in the adjacent coastal zones (Xu et al., 2018; Tang et al., 2021; Li et al., 2020).

River diversions at deltaic outlets are significant drivers of delta and coastal erosion. Abandoned delta lobes (sand spits) formed after such diversions are primary zones of terrestrial delta erosion (Jia et al., 2014). Since 1855, the Yellow River estuary has experienced over 50 diversions, with more than ten major events (Liu, 2017). Between 1964 and 1975, water and sediment supply to the abandoned Diaokou course steadily declined, with reductions of 48% and 40%, respectively, before the river's course was diverted in 1976. This resulted in a marked contraction of the river channel (Xing et al., 2016; Han et al., 2019). After 1976, the Diaokou course was abandoned. The Feiyan beach area, deprived of Yellow River sediments, experienced severe coastal erosion from 1984 to 2024, exacerbated by altered hydrodynamic conditions due to the construction of the Yellow River Port to the east (Wang et al., 2022). The most severe erosion in this region recorded rates of up to 121.54 m/a, with the coastline retreating as far as 4,861.64 m (Supplementary Table 6 and Figure 9).

In the first decade following the Yellow River's diversion to the Qingshuigou channel, there was an increase in water flow while the sediment load remained relatively stable. However, after 1986,

significant siltation occurred, causing channel contraction and deteriorating the water-sediment relationship. Post-1986, the water and sediment inflow dramatically decreased, dropping to only 44% and 48% of pre-1986 levels. In 1996, the river avulsed to the Qing 8 channel (Wu et al., 2021; Zhang and Hu, 2007), leaving the original Qingshuigou channel with minimal siltation due to residual water and sediment (Yu et al., 2016; Liu L. et al., 2023). After 2000, the Xiaolangdi Reservoir improved its water storage and sediment interception functions. Coupled with annual water and sediment regulation projects, the water-sediment dynamics at the Yellow River's estuary improved, enhancing the river's flow capacity and mitigating channel contraction. The original Qingshuigou channel's estuary experienced significant erosion from 2000 to 2015 (Cao et al., 2023). Although the water inflow remained stable, sediment inflow had reduced to only 28% of the pre-1999 levels. The rapid reduction in sediment supply prevented the original Qingshuigou channel from accumulating sufficient deposits, resulting in coastal erosion. After 2015, the rate of erosion stabilized. Meanwhile, the Q8 channel underwent straightening between 2011 and 2015, forming the current Yellow River channel. Continuous sediment supply from the Yellow River has led to the extension of the coastal line along the channel towards the northeast (Supplementary Table 7 and Figure 10).

## 4.2 Effects of extreme weather

Global warming has increased the frequency and intensity of extreme weather events, such as tropical cyclones and storm surges. The YRD, located in the northern part of the Shandong Peninsula, is particularly vulnerable to extreme hydrodynamic forces due to its long and meandering coastline bordered by seas on two sides (Qi et al., 2010). The impact of storm surges on tidal flats can vary depending on the storm's nature and the tidal flats' characteristics (Williams, 2009; Leonardi et al., 2018; Yang et al., 2019). Previous studies have shown that wave heights increase in the intertidal zone during storm surges, significantly contributing to the erosion of unvegetated tidal flats (Cahoon, 2006). Additionally, the high-velocity water flows induced by storm surges can resuspend surface sediments, increasing suspended sediment concentrations and enhancing sediment deposition during ebb tides or low-flow periods (Turner et al., 2007).

The primary driver of storm surges in the YRD is wind stress (Wu, 2017), with cold air, tropical cyclones, and extratropical cyclones being the direct causes (Huang, 2023). Storm surge warnings issued from 2014 to 2024 by the Dongying Marine Development and Fisheries Bureau (Dongying Municipal Bureau of Marine Development and Fisheries, 2014-2024) reveal that storm surges in the YRD predominantly occur from February to May and August to November. From January to May, storm surges are mainly caused by cold air, supplemented by extratropical cyclones, with an average water level rise of 98.95 cm, a minimum of 63.16 cm, and a maximum of 134.74 cm. Cold air-induced storm surges during this period average 95.83 cm, while combined cold air and extratropical cyclone-induced surges average

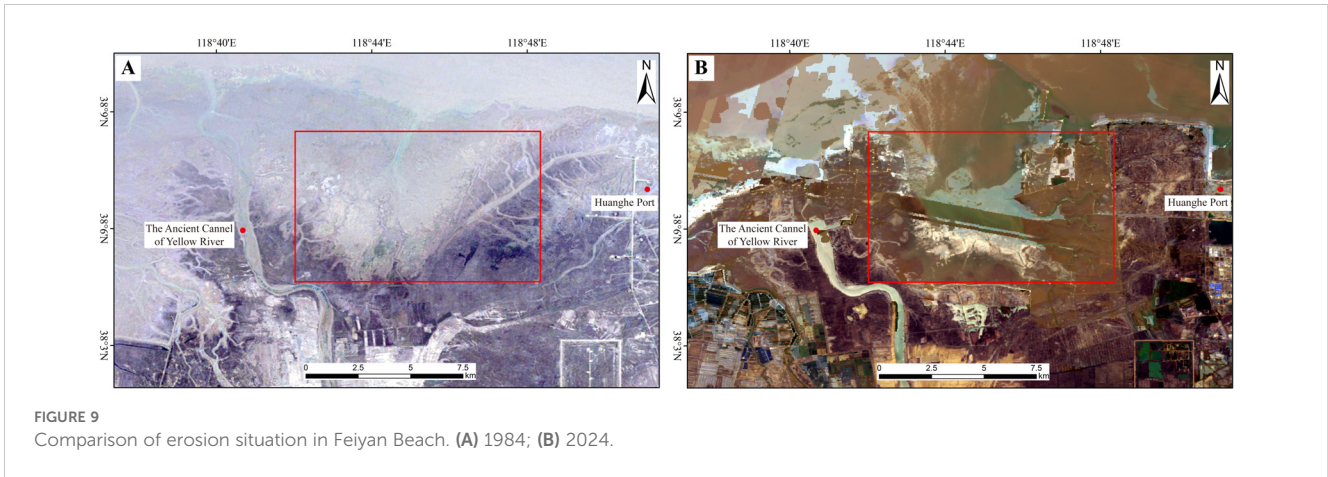


FIGURE 9 Comparison of erosion situation in Feiyan Beach. (A) 1984; (B) 2024.

104.29 cm, 8.46 cm higher than those caused solely by cold air. The situation becomes more complex from July to November, with tropical and extratropical cyclones causing storm surges in August and cold air or extratropical cyclones in September. From October to November, cold air and cold waves become the primary causes of storm surges in the YRD. From July to September, except for Typhoons Lekima in 2019 and Muifa in 2022, tropical cyclone-induced storm surges are relatively weak, averaging 70.17 cm, with a

maximum of 98.33 cm and a minimum of 42 cm. During this period, extratropical cyclone and cold air-induced surges are similar in intensity, averaging 82.5 cm and 72.5 cm, respectively. However, from October to November, cold air-dominated storm surges significantly increase in intensity, averaging 100.5 cm in October and 101.67 cm in November, and further rising to an average of 116.67 cm in December, 16 cm higher than in October. Overall, storm surge intensity in the YRD can be categorized by causative

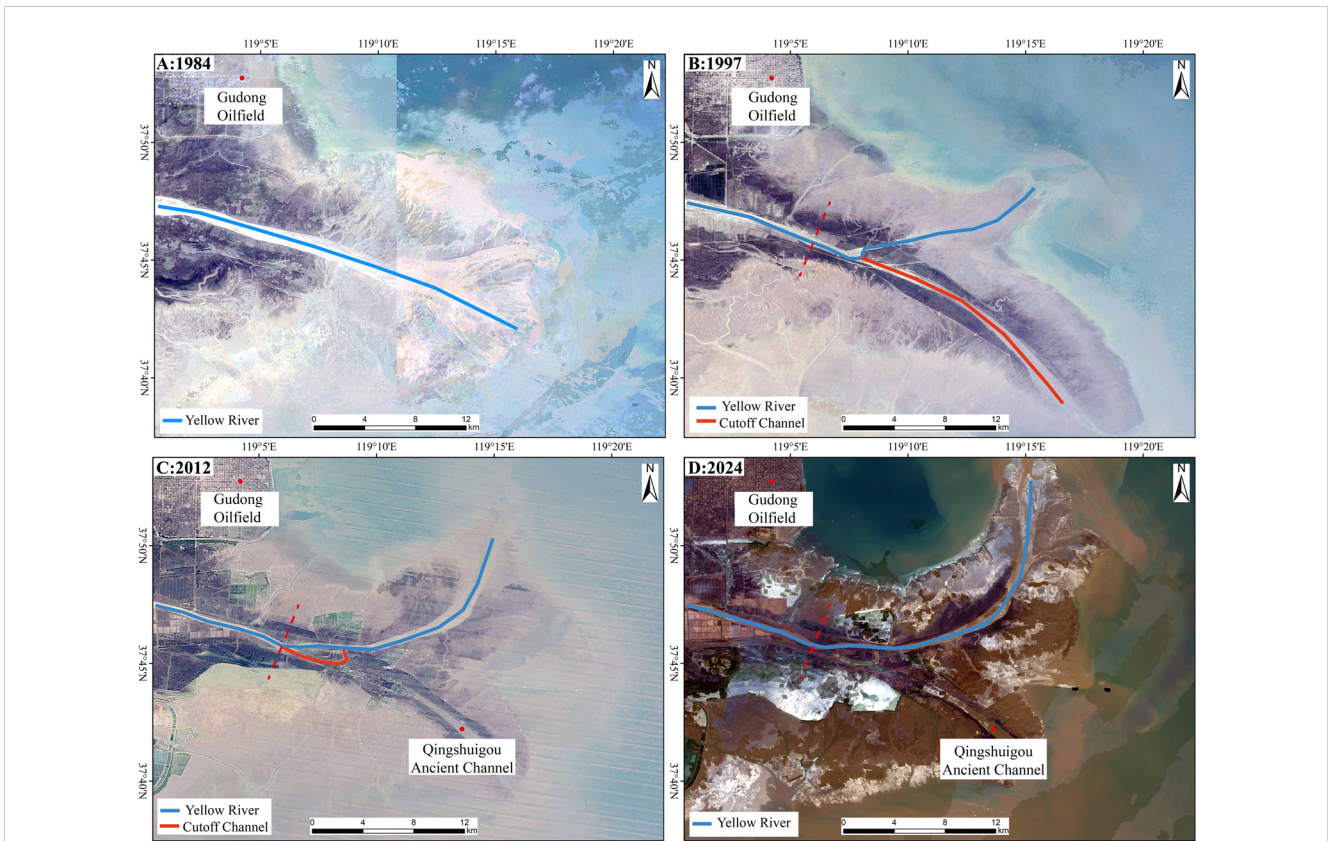


FIGURE 10 New and old Yellow River channels. (A) In 1984, the ancient channel extended continuously southeastward; (B) In 1996, the river changed the channel to the Qing 8 distributary, the new channel extended northeastward; (C) In 2012, the Q8 distributary underwent channel straightening; (D) In 2024, the new channel continues to extend northeastward, but the rate of coastline progradation has slowed.

factors: combined cold air and extratropical cyclone-induced surges have the highest average water level rise of 98.15 cm and are the primary natural factors affecting coastline erosion; extratropical cyclone-induced surges are next, with an average increase of 74 cm; and tropical storms, except for Typhoons Lekima and Muifa, have the lowest average rise of 63.5 cm (Figure 11 and Supplementary Table 8).

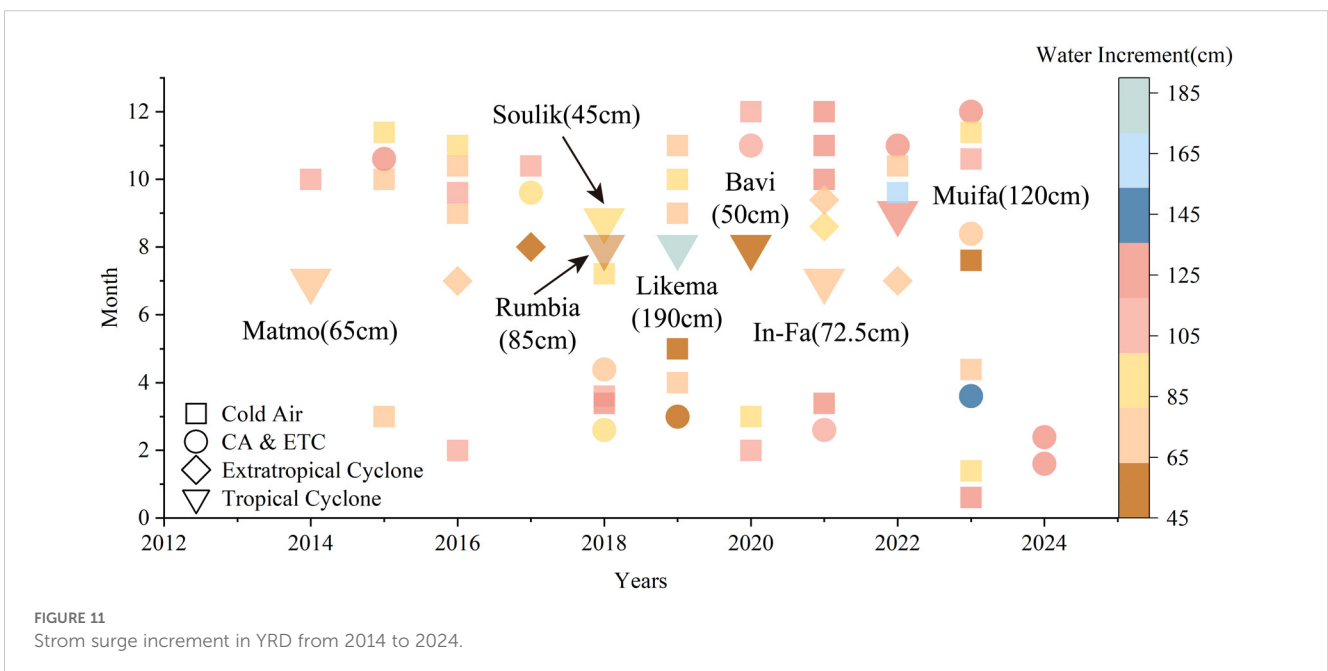
In the YRD, the impact of storm surges on topography is most pronounced in the erosion of the Gudong Oilfield's outer zone and the DK section to the north (Fan et al., 2018). By simulating the effects of century-scale storm surges under different wind directions using 1985 bathymetric data and comparing these results with 2015 topographic conditions, it was shown that between 1984 and 2015, erosion was concentrated near the seabed off the Gudong Oilfield and the Feiyan Beach region. Under the influence of northern and northeastern winds, the Diaokou River estuary area, particularly the Diaokou Ancient Channel and Feiyan Beach region, experienced maximum inundation distances of up to 18 km, with submerged areas ranging between 210 and 420 km<sup>2</sup> (Huang et al., 2022). In the SSP5-8.5 scenario, it is projected that the average inundation percentage along the YRD coastline will reach 48.5%, with coastal wetlands continuing to decline over the next century and severe coastal erosion expected to occur (Wang et al., 2024). The combined effects of extreme storm surge events, particularly when compounded by astronomical high tides, are expected to cause significant water level rises and intensify wave action in coastal regions, resulting in more substantial impacts on the coastline. Influenced by strong winter winds, the northern part of the YRD is particularly vulnerable. Consequently, the DK section and other north coastal sections are more prone to retreat due to erosion than the eastern sections. This trend aligns with the historical patterns of coastline erosion observed in the northern region of the delta (Supplementary Figure 1).

### 4.3 The joint impact of sea-level rise and delta subsidence

#### 4.3.1 Delta subsidence

Subsidence is a geological disaster characterized by the continual decline of surface elevation. Over 60 countries and regions worldwide have experienced ground subsidence (Törnqvist et al., 2008; Teatini et al., 2011), particularly in low-lying coastal delta areas. Most deltas worldwide are experiencing rapid subsidence, primarily driven by natural sediment deposition in river mouths and human activities. In the second half of the 20th century, the rapid expansion of urban areas and coastal engineering projects led to accelerated subsidence in many deltas. For example, the average subsidence rate in the Nile Delta was 2~50 mm/a (Stanley, 1990; Aly et al., 2012; Becker and Sultan, 2009). In the 21st century, subsidence rates in some deltas began to decrease as natural sediment consolidation increased. For instance, the average subsidence rate in the Mississippi River Delta dropped from 7.1~16.9 mm/a between 1969 and 1995 (Dixon et al., 2006) to 1~11 mm/a between 2010 and 2015 (Frederick et al., 2019; Jankowski et al., 2017). In contrast, the subsidence rate in the Chao Phraya River Delta has been increasing, with an average rate of 10~30 mm/a, twice that of previous years (Bhattacharya, 2013; Aobpaet et al., 2013). The primary driver of this increase is human activities, particularly groundwater extraction and urban development (Du et al., 2011; Bie et al., 2006), while the impact of natural factors on land subsidence has gradually diminished (Liu et al., 2011; Syvitski et al., 2009; Higgins, 2014).

Since the Bohai Bay earthquake in 1969, subsidence has been prevalent in the YRD region. Intense tectonic activity has led to continuous crustal subsidence, resulting in significant land settlement (The Geodetic Survey Bridge for Earthquake Research, National Seismological Bureau, 1977; Ye et al., 2021). Between 2007



and 2011, extreme subsidence values reached 250 mm/a, exceeding local and global average sea level rise rates by two orders of magnitude, making it the most severely subsiding delta worldwide (Higgins et al., 2014; Zhang et al., 2022). Subsidence in the YRD is distributed along both banks, with significant areas experiencing severe subsidence concentrated around Dongying City, the former river mouth, current river mouths, small towns, and oilfield regions. Subsidence rates are unevenly distributed, with localized areas showing rapid subsidence rates exceeding 300 mm/a (Huang et al., 1991; Li et al., 2000; Liu and Zhang, 2001; Xiao et al., 2003; Zhang et al., 2004; Bie et al., 2006). The impacts of ground subsidence may exacerbate catastrophic events such as coastal erosion, saltwater intrusion, and river flooding. The degree of coastal erosion in the YRD varies due to differences in sediment transport dynamics under the overarching context of subsidence (Supplementary Figure 3).

Historical subsidence data in the YRD demonstrates distinct temporal relationships with its coastline change:

#### 4.3.1.1 Rapid subsidence phase before 2000

From 1974 to 2000, the average subsidence rate in the YRD reached 50 to 53 mm/a, coinciding with a period of significant coastline change (Li et al., 2000; Du et al., 2011). In 1976, following the abandonment of the Diaokou River channel, the northern coastline of the delta lost a stable sediment supply. The newly deposited sediments underwent continuous compaction under their own weight, creating a rapid subsidence zone in the northern DK section, with an average subsidence rate of 5.8–15.6 mm/a (Zhang, 2015). Concurrently, due to global sea level rise and hydrodynamic actions, coastline erosion occurred rapidly, with an average coastline change rate of approximately -18.34 m/a. From 1976 to 1996, following the diversion of the Yellow River to the Qingshuigou channel, the influx of fresh water and sediment led to a subsidence rate of 5.7–22.6 mm/a (Liu and Huang, 2013; Chen R. R. et al., 2024). The continuous water and sediment supply mitigated the effects of terrestrial subsidence and sea level rise, resulting in a rapid coastal advance at the Qingshuigou estuary, with an average coastline change rate of 67.22 m/a (Supplementary Table S9).

#### 4.3.1.2 Transitional period from 2000 to 2015

Compared to pre-2000 subsidence rates, the subsidence rate in the YRD gradually slowed between 2000 and 2015, with the average rate decreasing to 20–30 mm/a. Nevertheless, this rate remains relatively high compared to other major river deltas globally (Fu Y. X. et al., 2021). During this period, the residual sediments of the northern Diaokou River channel, having undergone nearly 40 years of consolidation, exhibited significantly reduced subsidence rates, the average subsidence is 6 mm/a (Zhang et al., 2019). Coastal protection projects, such as the construction of coastal dikes, contributed to a gradual slowdown of erosion in the northern delta, with some areas beginning to show sedimentation, resulting in an average coastline change rate of 62.49 m/a. The eastern Qingshuigou channel, following the Yellow River's diversion in 1996, experienced a notable coastline retreat at an average change rate of -114.47 m/a due to a lack of sediment supply, compounded by sediment consolidation and sea

level rise. Conversely, new river mouths received sediment input, offsetting the effects of terrestrial subsidence and sea level rise, leading to a rapid coastal advance at an average change rate of 390.75 m/a (Supplementary Table 9).

#### 4.3.1.3 Stabilization period post-2015

Since 2015, the average subsidence rate in the YRD has further decreased to 0–36 mm/a, focusing on delta subsidence shifting inland (Ning et al., 2023; Zhang et al., 2022), and subsidence rates along the coastal regions have stabilized. During this period, the northern DK section and its surrounding areas exhibited sediment compaction rates of 80–90% (Liu et al., 2014), reaching high consolidation levels. This consolidation has gradually slowed subsidence rates and the completion of coastal protection projects has contributed to stabilizing coastline changes, with an average coastline change rate of -0.32 m/a. Following 2015, the subsidence rate in the eastern GN section decreased to 0 and 6 mm/a (Zhang et al., 2022, 2019). During this time, the water and sediment supply from the Yellow River has gradually diminished, leading to a further slowdown in the coastline change rate at the new river mouth, which now averages 118.23 m/a (Supplementary Table 9).

In summary, the interplay between relative sea level rise and ground subsidence primarily impacts the northern Diaokou River channel region of the YRD. In the early stages of the river path's cutoff, rapid compaction of fresh sediments resulted in pronounced subsidence and a rapid increase in relative sea level, leading to significant coastal erosion. As the degree of sediment compaction and consolidation increases and the focus of subsidence shifts inland, the ground subsidence rate at the DK section has stabilized. The coastline erosion caused by the relative sea level rise and ground subsidence has also gradually slowed. In contrast, the eastern GN section has benefited from continuous sediment input from the Yellow River, mitigating the combined impacts of relative sea level rise and ground subsidence, thereby allowing the coastline in the surrounding areas to continue advancing seaward.

### 4.3.2 Sea level rise

From 1901 to 2018, the global average sea level rose by 0.2 m. Since the 1970s, human-induced global warming, glacier melting, and thermal expansion of seawater have emerged as the primary factors accelerating sea level rise. Currently, the global sea level rise rate is approximately 2.3 mm/a, and it is projected to continue accelerating for the foreseeable future. This trend directly impacts the ecological environment, economy, and social life in delta regions and their surroundings (IPCC, 2023).

Relative sea level changes have extensive implications for delta regions. Rising sea levels not only affect surface water flow in deltas but also increase the likelihood of flooding, including storm surges and river floods (Moftakhari et al., 2017). Predictions from the global delta and relative sea level rise database indicate that by 2300, approximately 85% of global deltas may face over 10 km<sup>2</sup> of land being forced into a state of inundation (Nienhuis and Van de Wal, 2021). By the end of the 21st century, if protective measures are not implemented, an estimated 2,660 square kilometers of land in the Nile Delta could be submerged by seawater (Gebremichael et al., 2018).

In the Niger Delta, the coastline retreated due to rising sea levels reached a maximum of 17 km between 1991 and 2018 (Abija et al., 2020). Without human intervention, estimates suggest that rising sea levels could cause a coastline retreat of between 80 and 600 meters in the Danube Delta (Stănică et al., 2011; Stănică and Panin, 2009). In the context of rising sea levels, extreme wave events over the next century could lead to approximately 4 km of coastal erosion in the Nile Delta (El-Mahdy et al., 2022).

Simultaneously, sea level rise elevates wave action and tidal limits, resulting in increased erosion base levels. Profiles that were previously in equilibrium cannot adapt to these new dynamic conditions, leading to the formation of new profiles and altering coastal sediment processes, which in turn triggers coastal erosion (Anderson et al., 2015; Bonaldo et al., 2019). Since 1980, the rate of sea level rise in the YRD region has been 3.8 mm/a (China Sea Level Bulletin, 2023) (Supplementary Figure 2). Data from tide gauge measurements and precise leveling along the Bohai Sea coast and the Shandong Peninsula indicate that the relative sea level rise in the YRD is primarily driven by land subsidence, which is further exacerbated by the rise in sea levels (Bondesan and Simenoi, 1983; Abam, 2001; Syvitski et al., 2009). The combined effects of sea level rise and land subsidence heighten the flood risk and coastal erosion in the YRD region, with seasonal coastal flooding resulting in a net erosion rate of  $0.07 \times 10^8 \text{ m}^2/\text{a}$  and maximum erosion depths in abandoned river mouth areas reaching 7 km (Fu et al., 2023).

#### 4.4 The impact of human activities

The historical evolution of coastal zones has been driven by interactions among terrestrial, marine, fluvial, and atmospheric factors. However, since the Industrial Revolution, the intensity and speed of coastal modifications due to human activities have far surpassed natural processes. Consequently, human activities are considered the “third driving force” after the Earth’s internal energy and solar energy (McLaren et al., 2024; Xu L. et al., 2014). These activities affect the geomorphology of coastal regions and influence the sediment load rivers carry to the sea. The construction of reservoirs, water diversions, and increased water consumption in the Yellow River basin have controlled the water and sediment flow into the sea, thereby impacting the erosion and deposition patterns along the YRD’s coastline (Briceño De Urbaneja et al., 2024; Yi, 2011).

Human activities in the study area include marine aquaculture, coastal dam construction, port engineering, and resource extraction projects. These land reclamation activities have accounted for 88.72% of the expansion of tidal flats in the YRD. Since the 1980s, the region has seen extensive development of marine aquaculture, with the construction of numerous shrimp, fish, and salt ponds. Additionally, land reclamation projects occupy a large number of original mudflats, causing the coastline to expand rapidly to the seaward (Zhan et al., 2023). Between 1984 and 2024, the area of aquaculture ponds expanded to 784.00 km<sup>2</sup>, comprising 74.6% of the total reclaimed land. Port engineering

projects, including those at Huanghua Port, Guangli Port, and Yellow River Port, have significantly altered the hydrodynamic conditions around these ports. Over the past 40 years, the area dedicated to port engineering reached 171.51 km<sup>2</sup> or 16.33% of the total reclaimed land. The construction of the Yellow River Port solidified the coastline in the northeast of the YRD, preventing sediment from migrating northward, thus directly or indirectly causing severe erosion of the Feiyan Beach coastline. The Gudong Oilfield, located between Yellow River Port and the Qingshuigou estuary, is the most significant resource extraction project in the YRD. Since its main coastal construction was completed in 1987, the oilfield area has shifted from horizontal to vertical erosion to the dam downwards. The total area of coastal engineering projects, including the oilfield, reached 95.08 km<sup>2</sup>, accounting for 9.05% of the total reclaimed land (Figure 12).

The extensive land reclamation projects have rapidly extended the coastline and altered its characteristics. Over the past 40 years, natural coastlines have been rapidly transformed into artificial coastlines. In the study area, four typical coastal sections exhibit consistent trends in coastline changes. The most significant transformations have occurred in the XB and DK sections, where the proportion of artificial coastline increased from 10.33% and 13.21% to 93.44% and 95.64%, respectively. The GL section saw a smaller increase of 62.17% in the artificial coastline from 1984 to 2024. The GN section also experienced a smaller increase, with the proportion of artificial coastline rising from 18.85% in 1984 to 57.30% in 2024. This smaller increase is attributed to the continuous sediment deposition from the Yellow River, which extended the natural coastline at the new and old estuaries (Zhan et al., 2020), thereby increasing the total length of the coastline and making the increment of the artificial coastline relatively smaller (Figure 13).

## 5 Conclusions

(1) From 1984 to 2024, Between 1984 and 2024, the coastline of the Yellow River Delta underwent three distinct stages of change: rapid transformation, gradual slowdown, and eventual stabilization. Each stage lasted approximately 15 years. During this period, the coastline as a whole prograded seawards, with artificial shorelines formed by land reclamation and other engineering projects gradually becoming the dominant feature of the modern Yellow River Delta coastline. Notably, the abandoned estuary of the Diao Kou River and the active estuary of the Qingshuigou River exhibited both erosion and deposition, while other sections of the coastline showed either accretion or stability.

(2) The river’s avulsion primarily influenced early Yellow River Delta coastline changes. However, following the stabilization of the Qingshuigou channel, natural factors such as global climate warming, land subsidence, and extreme weather events became the main drivers of coastline change. Among these, the relative sea-level rise caused by global warming and land subsidence has exacerbated coastal erosion, but its impact remains relatively small. In contrast, the increased frequency of extreme storm

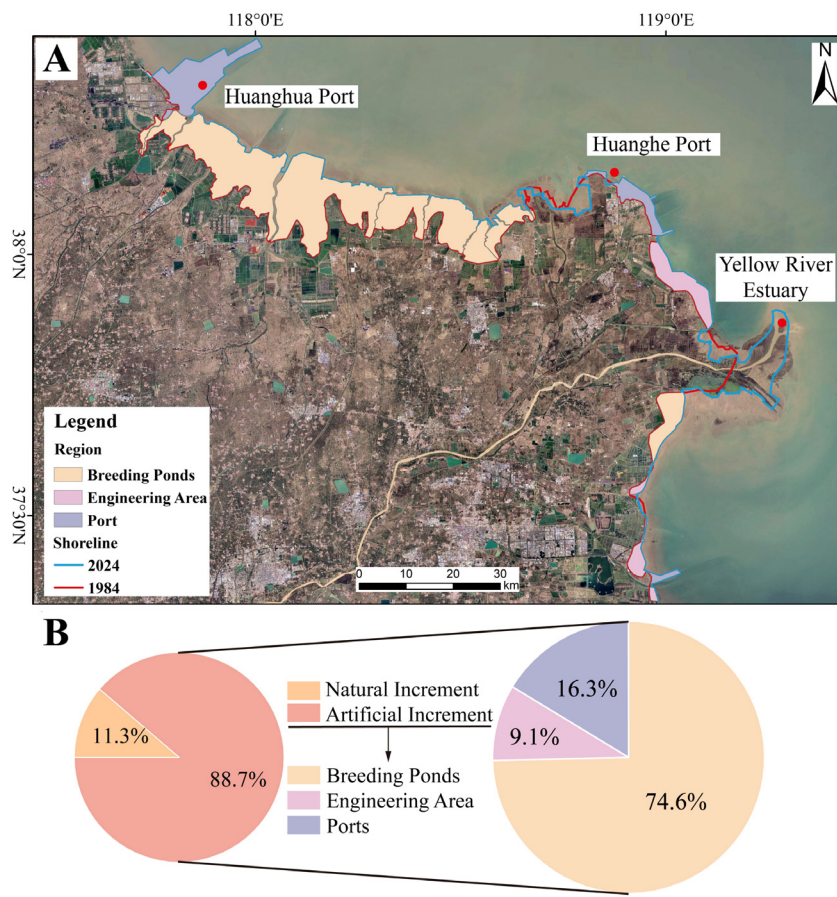


FIGURE 12 Types and area of artificial reclamation from 1984 to 2024. (A) Land reclamation area; (B) The proportion of natural increment and artificial increment.

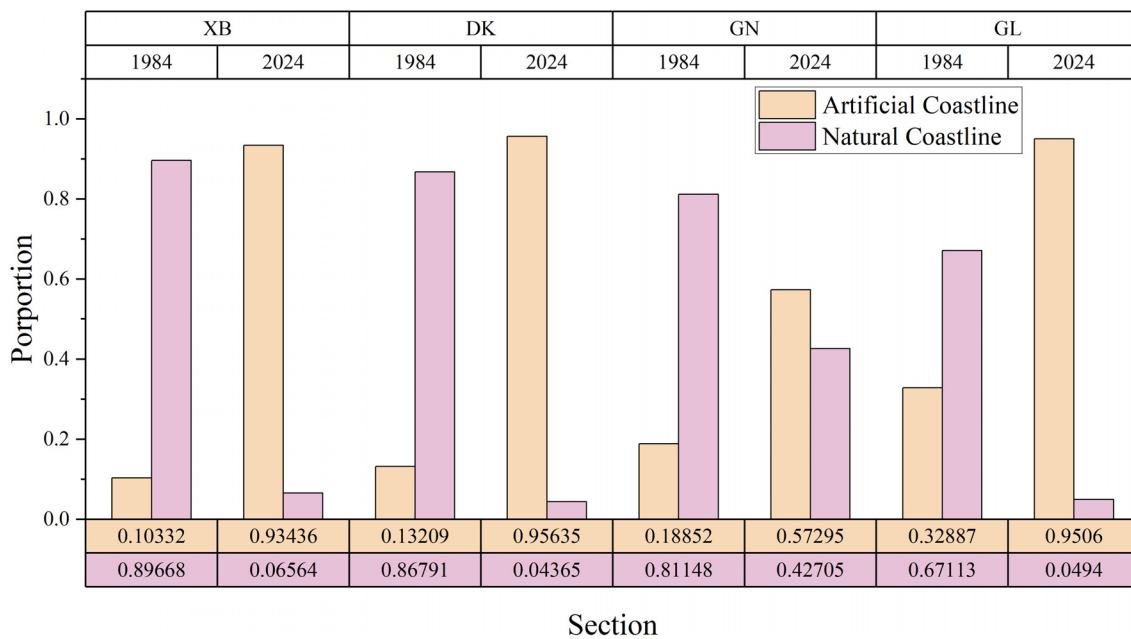


FIGURE 13 The proportion of different types of coastlines in each typical section.

surges driven by climate change has significantly impacted the coastline of YRD, especially in the northern parts of the delta.

(3) Compared to other deltas, the YRD experiences a combination of factors, including high subsidence rates, frequent river course shifts, intense extreme weather events, and extensive human activities, all contributing to its highly complex coastline changes. The impacts of local hydrodynamic changes and variations in coastline utilization are mainly more pronounced. The patterns of coastline change vary significantly across different types of coastline segments, such as abandoned river mouths, active river mouths, and areas of human development.

## Data availability statement

The original contributions presented in the study are included in the article/Supplementary Material. Further inquiries can be directed to the corresponding author/s.

## Author contributions

ZY: Data curation, Methodology, Validation, Writing – original draft, Writing – review & editing. WG: Conceptualization, Data curation, Funding acquisition, Methodology, Project administration, Resources, Supervision, Validation, Writing – review & editing. WY: Data curation, Writing – review & editing. JL: Data curation, Writing – review & editing. JD: Project administration, Writing – review & editing. PL (6th author): Project administration, Writing – review & editing. YX: Project administration, Writing – review & editing. PL (8th author): Writing – review & editing.

## Funding

The author(s) declare financial support was received for the research, authorship, and/or publication of this article. This research is supported by the National Key Research and Development Program of China (Grant Number 2022YFC3106100) and the Shandong Provincial Natural Science Foundation, China (Grant Number ZR2021MD098).

## Conflict of interest

The authors declare that the research was conducted in the absence of any commercial or financial relationships that could be construed as a potential conflict of interest.

## Publisher's note

All claims expressed in this article are solely those of the authors and do not necessarily represent those of their affiliated organizations, or those of the publisher, the editors and the reviewers. Any product that may be evaluated in this article, or claim that may be made by its manufacturer, is not guaranteed or endorsed by the publisher.

## Supplementary material

The Supplementary Material for this article can be found online at: <https://www.frontiersin.org/articles/10.3389/fmars.2024.1490990/full#supplementary-material>

### SUPPLEMENTARY FIGURE 1

Inundation depth variations in 100-year return period wind in different directions.

### SUPPLEMENTARY FIGURE 2

The trend of Sea-Level changes in the north of Yangtze River from 1980 to 2022.

### SUPPLEMENTARY FIGURE 3

Variation of surface ground subsidence rate with time in Yellow River Delta.

### SUPPLEMENTARY TABLE 1

The format and source of remote sensing images.

### SUPPLEMENTARY TABLE 2

XB section NSM & EPR data.

### SUPPLEMENTARY TABLE 3

DK section NSM & EPR data.

### SUPPLEMENTARY TABLE 4

GN section NSM & EPR data.

### SUPPLEMENTARY TABLE 5

GL section NSM & EPR data.

### SUPPLEMENTARY TABLE 6

Water and sediment inflow from Lijin Station from 1964 to 1975.

### SUPPLEMENTARY TABLE 7

Water and sediment inflow from Lijin Station from 1976 to 2020.

### SUPPLEMENTARY TABLE 8

Strom surge increment data in Yellow River Delta form 2014 to 2024.

### SUPPLEMENTARY TABLE 9

Land subsidence rate in major river deltas worldwide. References (Huang et al., 2022; Zhang et al., 2019, 2022; Dixon et al., 2006; Syvitski et al., 2009; Ivins et al., 2007; Törnqvist et al., 2008; Frederick et al., 2019; Jankowski et al., 2017; Alam, 1996; Goodbred and Kuehl, 2000; Higgins et al., 2014; Stanley, 1990; Aly et al., 2012; Becker and Sultan, 2009; Rateb and Abotalib, 2020; Gambolati et al., 1999; Erban et al., 2014; Teatini et al., 2011; Bhattacharya, 2013; Aobpaet et al., 2013; Wang et al., 2012; Ren et al., 2024; Xiong and Zhu, 2007; Chen Y. et al., 2024; Li et al., 2000; Du et al., 2011; Liu et al., 2014; Fu et al., 2021; Ning et al., 2023) are cited in the Supplementary Materials.

## References

- Abam, T. K. S. (2001). Regional hydrological research perspectives in the Niger Delta. *Hydrological Sci. J.* 46, 13–25. doi: 10.1080/02626660109492797
- Abija, F., Abam, T., and Eze, C. (2020). *Relative sea level rise, coastline variability and coastal erosion in the niger delta, nigeria: Implications for climate change adaptation and coastal zone management*, Vol. 11.
- Abou Samra, R. M., and Ali, R. R. (2021). Applying DSAS tool to detect coastal changes along Nile Delta, Egypt. *Egyptian J. Remote Sens. Space Sci.* 24, 463–470. doi: 10.1016/j.ejrs.2020.11.002
- Alam, M. (1996). "Subsidence of the Ganges-Brahmaputra Delta of Bangladesh and associated drainage, sedimentation and salinity problems," in *the sea-level rise and coastal subsidence: causes, consequences and strategies*. Eds. J. D. Milliman and B. U. & Haq (Kluwer Academic, Dordrecht), 169–187.
- Alber, A., and Piégay, H. (2017). Characterizing and modelling river channel migration rates at a regional scale: Case study of south-east France. *J. Environ. Manage.* 202, 479–493. doi: 10.1016/j.jenvman.2016.10.055
- Aleshikh, A. A., Ghorbanali, A., and Nouri, N. (2007). Coastline change detection using remote sensing. *Int. J. Environ. Sci. Technol.* 4, 61–66. doi: 10.1007/BF03325962
- Aly, M. H., Klein, A. G., Zebker, H. A., and Giardino, J. R. (2012). Land subsidence in the Nile Delta of Egypt observed by persistent scatterer interferometry. *Remote Sens. Lett.* 3, 621–630. doi: 10.1080/01431161.2011.652311
- Anderson, T. R., Fletcher, C. H., Barbee, M. M., Frazer, L. N., and Romine, B. M. (2015). Doubling of coastal erosion under rising sea level by mid-century in Hawaii. *Nat. Hazards* 78, 75–103. doi: 10.1007/s11069-015-1698-6
- Aobpaet, A., Cuenca, M. C., Hooper, A., and Trisirisatayawong, I. (2013). InSAR time-series analysis of land subsidence in Bangkok, Thailand. *Int. J. Remote Sens.* 34, 2969–2982. doi: 10.1080/01431161.2012.756596
- Avoronyo, S. Y., Appeaning Addo, K., Teatini, P., Minderhoud, P., Willez, M.-N., Jayson-Quashigah, P.-N., et al. (2023). A scoping review of coastal vulnerability, subsidence and sea level rise in Ghana: Assessments, knowledge gaps and management implications. *Quaternary Sci. Adv.* 12, 100108. doi: 10.1016/j.qsa.2023.100108
- Becker, R. H., and Sultan, M. (2009). Land subsidence in the Nile Delta: inferences from radar interferometry. *Holocene* 19, 949–954. doi: 10.1177/0959683609336558
- Bhattacharya, A. K. (2013). An analysis of land subsidence in Bangkok and Kolkata due to over-extraction of groundwater. *Electronic J. Geotechnical Eng.* 18, 1683–1694.
- Bianchi, T. S., Schreiner, K. M., Smith, R. W., Burdige, D. J., Woodard, S., and Conley, D. J. (2016). Redox effects on organic matter storage in coastal sediments during the holocene: A Biomarker/Proxy perspective. *Annu. Rev. Earth Planet. Sci.* 44, 295–319. doi: 10.1146/annurev-earth-060614-105417
- Bie, J., Huang, H. J., and Fan, H. (2006). Ground subsidence of the modern Yellow River Delta and its causes. *Mar. Geology Quaternary Geology* 26, 29–35. doi: 10.16562/j.cnki.0256-1492.2006.04.005
- Bonaldo, D., Antonioli, F., Archetti, R., Bezzi, A., Correggiari, A., Davolio, S., et al. (2019). Integrating multidisciplinary instruments for assessing coastal vulnerability to erosion and sea level rise: lessons and challenges from the Adriatic Sea, Italy. *J. Coast. Conserv.* 23, 19–37. doi: 10.1007/s11852-018-0633-x
- Bondesan, M., and Simeoni, V. (1983). Dinamica e analisi morfologica statistica dei litorali del delta del Po e alle foci dell'Adige e del Brenta. *Memorie degli Istituti di Geologia e Mineralogia dell'Università di Padova.* 36, 1–48
- Briceño De Urbaneja, I. C., Pardo-Pascual, J. E., Cabezas-Rabadán, C., Aguirre, C., Martínez, C., Pérez-Martínez, W., et al. (2024). Characterization of multi-decadal beach changes in cartagena bay (Valparaiso, Chile) from satellite imagery. *Remote Sens.* 16, 2360. doi: 10.3390/rs16132360
- Cahoon, D. R. (2006). A review of major storm impacts on coastal wetland elevations. *Estuaries Coasts* 29, 889–898. doi: 10.1007/BF02798648
- Cao, Y., Wang, Q., Zhan, C., Li, R., Qian, Z., Wang, L., et al. (2023). Evolution of tidal flats in the Yellow River Qingshuigou sub-delta: spatiotemporal analysis and mechanistic changes (1996–2021). *Front. Mar. Sci.* 10. doi: 10.3389/fmars.2023.1286188
- Chen, R. R., Sun, H. Y., Zhu, Z. R., Jiang, X. Z., Chen, S. L., and Chen, J. (2024). Research progress and future prospects of land subsidence in the Yellow River Delta. *Coast. Eng.* 43, 1–23.
- Chen, S. L., Zhang, G. A., and Gu, G. C. (2004). Mechanism of heavy coastal erosion on Yellow River Delta and its countermeasures. *J. Hydraulic Eng.* 07, 1–6+13.
- Chen, X., Hu, C., and An Y. Q. (2021). Research on the reasonable allocation scheme of sediment in the Yellow River. *J. Sediment Res.* 46, 1–9.
- Chen, Y., Guo, L., Xu, J., Yang, Q., Wang, H., and Zhu, C. (2024). Monitoring and cause analysis of land subsidence along the yangtze river utilizing time-series inSAR. *IJGI* 13, 230. doi: 10.3390/ijgi13070230
- China Sea Level Bulletin. (2023). *China oceanic information network*. Available online at: <https://www.nmdis.org.cn/hygb/zghpmb> (Accessed July 15, 2024).
- Chu, Z., Ma, X., Zhang, J., Dong, M., and Gao, Y. (2005). Comparison of mean high tide line and 2 m isobath reflecting erosion and accretion of the Yellow River Delta. *Mar. Geol. Quaternary Geol.* 25, 23. doi: 10.16562/j.cnki.0256-1492.2005.04.004
- Chu, L., Oloo, F., Sudmanns, M., Tiede, D., Hölbling, D., Blaschke, T., et al. (2020). Monitoring long-term shoreline dynamics and human activities in the Hangzhou Bay, China, combining daytime and nighttime EO data. *Big Earth Data* 4, 242–264. doi: 10.1080/20964471.2020.1740491
- Day, J. W., Twilley, R. R., Freeman, A., Couvillion, B., Quirk, T., Jafari, N., et al. (2023). The concept of land bridge marshes in the Mississippi River Delta and implications for coastal restoration. *Nature-Based Solutions* 3, 100061. doi: 10.1016/j.nbsj.2023.100061
- Dixon, T. H., Amelung, F., Ferretti, A., Novali, F., Rocca, F., Dokka, R., et al. (2006). Subsidence and flooding in new orleans. *Nature* 441, 587–588. doi: 10.1038/441587a
- Donchyts, G., Schellekens, J., Winsemius, H., Eisemann, E., and Van De Giesen, N. (2016). A 30 m resolution surface water mask including estimation of positional and thematic differences using landsat 8, SRTM and openStreetMap: A case study in the murray-darling basin, Australia. *Remote Sens.* 8, 386. doi: 10.3390/rs8050386
- Dong, W. S., Ariffin, E. H., Saengsupavanich, C., Mohd Rashid, M. A., Mohd Shukri, M. H., Ramli, M. Z., et al. (2023). Adaptation of coastal defence structure as a mechanism to alleviate coastal erosion in monsoon dominated coast of Peninsular Malaysia. *J. Environ. Manage.* 333, 117391. doi: 10.1016/j.jenvman.2023.117391
- Dongying Municipal Bureau of Marine Development and Fisheries (2014–2024). Available online at: <http://hsdy.dongying.gov.cn> (Accessed July 15, 2024).
- Du, T. Q., Huang, H. J., and Bie, J. (2011). Land subsidence in the modern Yellow River Delta and its impacts upon its evolution. *Mar. Sci.* 35, 78–84.
- Duan, P., Li, J., Wang, M., and Wu, J. (2021). Spatial-temporal analysis of the coastline changes in Fujian province, China from 1995 to 2015. *JESAM* 24, 1–9. doi: 10.47125/jesam/2021\_2/01
- Edmonds, D. A., Caldwell, R. L., Brondizio, E. S., and Siani, S. M. O. (2020). Coastal flooding will disproportionately impact people on river deltas. *Nat. Commun.* 11, 4741. doi: 10.1038/s41467-020-18531-4
- El-Mahdy, M. E.-S., Saber, A., Moursy, F. E., Sharaky, A., and Saleh, N. (2022). Coastal erosion risk assessment and applied mitigation measures at ezbet elborg village, egyptian delta. *Ain Shams Eng. J.* 13, 101621. doi: 10.1016/j.asej.2021.10.016
- Erban, L. E., Gorelick, S. M., and Zebker, H. A. (2014). Groundwater extraction, land subsidence, and sea-level rise in the Mekong Delta, Vietnam. *Environ. Res. Lett.* 9, 84010. doi: 10.1088/1748-9326/9/8/084010
- Fan, Y. S. (2019). *Seabed erosion and its mechanism in the littoral area of Yellow River Delta*. [PhD thesis] (Shanghai: East China Normal University).
- Fan, Y., Chen, S., Zhao, B., Pan, S., Jiang, C., and Ji, H. (2018). Shoreline dynamics of the active Yellow River delta since the implementation of Water-Sediment Regulation Scheme: A remote-sensing and statistics-based approach. *Estuarine Coast. Shelf Sci.* 200, 406–419. doi: 10.1016/j.ecss.2017.11.035
- Frederick, B. C., Blum, M., Fillon, R., and Roberts, H. (2019). Resolving the contributing factors to Mississippi Delta subsidence: Past and Present. *Basin Res.* 31, 171–190. doi: 10.1111/bre.12314
- Fu, S. (2020). Biodiversity conservation along the Yellow River should emphasize the complex spatial heterogeneity. *Biodiversity Sci.* 28, 1445–1446. doi: 10.17520/biods.2021003
- Fu, Y., Bellerby, R. G. J., Ji, H., Chen, S., Fan, Y., and Li, P. (2023). Impacts of riverine floods on morphodynamics in the yellow river delta. *Water* 15, 1568. doi: 10.3390/w15081568
- Fu, Y., Chen, S., Ji, H., Fan, Y., and Li, P. (2021). The modern Yellow River Delta in transition: Causes and implications. *Mar. Geology* 436, 106476. doi: 10.1016/j.margeo.2021.106476
- Fu, Y. X., Guan, Y., and Wang, X. D. (2021). Research on land subsidence mechanisms of mega-river deltas: taking the Yellow River Delta as the case. *Coast. Eng.* 40, 83–95.
- Gambolati, G., Teatini, P., Tomasi, L., and Gonella, M. (1999). Coastline regression of the Romagna Region, Italy, due to natural and anthropogenic land subsidence and sea level rise. *Water Resour. Res.* 35, 163–184. doi: 10.1029/1998WR900031
- Gao, W. (2011). *Stratigraphy sequence of Diaokou lobe in the modern Yellow River Delta*. [PhD thesis] ([Shandong]: Ocean University of China).
- Gao, W., Du, J., Gao, S., Xu, Y., Li, B., Wei, X., et al. (2023). Shoreline change due to global climate change and human activity at the Shandong Peninsula from 2007 to 2020. *Front. Mar. Sci.* 9. doi: 10.3389/fmars.2022.1123067
- Gao, W., Liu, S., Liu, J., Xu, Y., and Li, P. (2018). The sedimentary facies and dynamic environment of the Diaokou lobe in the modern Huanghe River Delta of China. *Acta Oceanol. Sin.* 37, 40–52. doi: 10.1007/s13131-018-1332-z
- Gao, W., Liu, J., Xu, Y., and Li, P. (2024). Evolution of sandy shores under the combined impact of global climate change and anthropogenic activities in Shandong Peninsula, East China. *J. Asian Earth Sci.* 259, 105887. doi: 10.1016/j.jseas.2023.105887
- Gebremichael, E., Sultan, M., Becker, R., El Bastawesy, M., Cherif, O., and Emil, M. (2018). Assessing land deformation and sea encroachment in the Nile delta: A radar interferometric and inundation modeling approach. *JGR Solid Earth* 123, 3208–3224. doi: 10.1002/2017JB015084
- Goodbred, S. L., and Kuehl, S. A. (2000). The significance of large sediment supply, active tectonism, and eustasy on margin sequence development: Late Quaternary

- stratigraphy and evolution of the Ganges–Brahmaputra delta. *Sedimentary Geology* 133, 227–248. doi: 10.1016/S0037-0738(00)00041-5
- Han, S. S., Zheng, S., and Tan, G. M. (2019). Comparison of fluvial processes on Qingshuigou and Diaokouhe Channels in the Yellow River Delta. *J. Sediment Res* 44, 27–32. doi: 10.16239/j.cnki.0468-155x.2019.06.005
- Higgins, S. (2014). *River delta subsidence measured with interferometric synthetic aperture radar (InSAR)*. [PhD thesis] (Boulder: University of Colorado).
- Higgins, S. A. (2016). Review: Advances in delta-subsidence research using satellite methods. *Hydrogeol J* 24, 587–600. doi: 10.1007/s10040-015-1330-6
- Higgins, S. A., Overeem, I., Steckler, M. S., Syvitski, J. P. M., Seeber, L., and Akhter, S. H. (2014). InSAR measurements of compaction and subsidence in the Ganges–Brahmaputra Delta, Bangladesh. *JGR Earth Surface* 119, 1768–1781. doi: 10.1002/2014JF003117
- Huang, L. (2023). *Impact of storm surge on the yellow river delta: simulation and analysis*. [master's thesis]. (Shanghai: East China Normal University).
- Huang, L., Chen, S., Pan, S., Li, P., and Ji, H. (2022). Impact of storm surge on the yellow river delta: simulation and analysis. *Water* 14, 3439. doi: 10.3390/w14213439
- Huang, L. R., Hu, H. M., and Yang, G. H. (1991). Sea level change along the western and south coast of Bohai and recent crustal vertical movement in adjacent area. *Crustal Deformation Earthquake* 11, 1–9.
- IPCC (2023). *Climate change 2023: synthesis report. Contribution of working groups I, II and III to the sixth assessment report of the intergovernmental panel on climate change*. Eds. C. W. Team, H. Lee and J. Romero (Geneva, Switzerland: IPCC), 184. doi: 10.59327/IPCC/AR6-9789291691647
- Ivins, E. R., Dokka, R. K., and Blom, R. G. (2007). Post-glacial sediment load and subsidence in coastal Louisiana. *Geophysical Res. Lett* 34, 2007GL030003. doi: 10.1029/2007GL030003
- Jankowski, K. L., Törnqvist, T. E., and Fernandes, A. M. (2017). Vulnerability of Louisiana's coastal wetlands to present-day rates of relative sea-level rise. *Nat. Commun* 8, 14792. doi: 10.1038/ncomms14792
- Ji, H., Chen, S., Pan, S., Xu, C., Tian, Y., Li, P., et al. (2022). Fluvial sediment source to sink transfer at the Yellow River Delta: Quantifications, causes, and environmental impacts. *J. Hydrology* 608, 127622. doi: 10.1016/j.jhydrol.2022.127622
- Jia, Y., Zheng, J., Yue, Z., Liu, X., and Shan, H. (2014). Tidal flat erosion of the Huanghe River Delta due to local changes in hydrodynamic conditions. *Acta Oceanol. Sin* 33, 116–124. doi: 10.1007/s13131-014-0501-y
- Kim, M. K., Sohn, H. G., Kim, S. P., and Jang, H. S. (2013). Automatic coastline extraction and change detection monitoring using LANDSAT imagery. *J. Korean Soc. Geospatial Inf. System* 21, 45–53. doi: 10.7319/kogsis.2013.21.4.045
- Kong, D., Miao, C., Borthwick, A. G. L., Duan, Q., Liu, H., Sun, Q., et al. (2015). Evolution of the Yellow River Delta and its relationship with runoff and sediment load from 1983 to 2011. *J. Hydrology* 520, 157–167. doi: 10.1016/j.jhydrol.2014.09.038
- Leonardi, N., Carnacina, I., Donatelli, C., Ganju, N. K., Plater, A. J., Schuerch, M., et al. (2018). Dynamic interactions between coastal storms and salt marshes: A review. *Geomorphology* 301, 92–107. doi: 10.1016/j.geomorph.2017.11.001
- Li, P., Wang, G., Liang, C., Wang, H., and Li, Z. (2023). InSAR-derived coastal subsidence reveals new inundation scenarios over the yellow river delta. *IEEE J. Sel. Top. Appl. Earth Observations Remote Sens* 16, 8431–8441. doi: 10.1109/JSTARS.2023.3272782
- Li, Z., Wang, H., Nittrouer, J. A., Bi, N., Wu, X., and Carlson, B. (2020). Modeling the infilling process of an abandoned fluvial-deltaic distributary channel: An example from the Yellow River delta, China. *Geomorphology* 361, 107204. doi: 10.1016/j.geomorph.2020.107204
- Li, M. L., Wu, S. L., and Gong, X. L. (2022). Characteristics of coastline change under the influence of human activities in central Jiangsu Province from 1989 to 2019. *Mar. Sci* 46, 60–68. doi: 10.11759/hyxx/20210512003
- Li, K., Zhang, L., Chen, B., Zuo, J., Yang, F., and Li, L. (2023). Analysis of China's coastline changes during 1990–2020. *Remote Sens* 15, 981. doi: 10.3390/rs15040981
- Li, G. X., Zhuang, K. L., and Jiang, Y. C. (2000). Engineering instability of the deposition bodies in the Yellow River Delta. *Mar. Geology Quaternary Geology* 20, 21–26. doi: 10.16562/j.cnki.0256-1492.2000.02.004
- Liu, J. W., Huang, H. J., Du, Q. T., Bie, J., and Chen, J. T. (2011). Effective factors of land subsidence in the yellow river delta. *Mar. Sci.* 35, 43–50.
- Liu, Y. B. (2017). *Diversion of the Yellow River and its influence on delta wetland evolution research*. [master's thesis] (Shandong: Shandong Normal University).
- Liu, X. X. (2022). *Coastal evolution and its influencing factors of Qingshuigou lobe in the Yellow River Delta*. [master's thesis] (Shandong: East China Normal University).
- Liu, S., Feng, A., Du, J., Xia, D., Li, P., Xue, Z., et al. (2014). Evolution of the buried channel systems under the modern Yellow River Delta since the Last Glacial Maximum. *Quaternary Int* 349, 327–338. doi: 10.1016/j.quaint.2014.06.061
- Liu, Y., and Huang, H.-J. (2013). Characterization and mechanism of regional land subsidence in the Yellow River Delta, China. *Nat. Hazards* 68, 687–709. doi: 10.1007/s11069-013-0648-4
- Liu, H., and Jezek, K. C. (2004). Automated extraction of coastline from satellite imagery by integrating Canny edge detection and locally adaptive thresholding methods. *Int. J. Remote Sens* 25, 937–958. doi: 10.1080/0143116031000139890
- Liu, L., Ji, P. F., and Shi, H. L. (2023). Variation of flow and sediment and evolution response in the Qingshuigou channel of the Yellow River Estuary. *J. Sediment Res* 48, 70–74. doi: 10.16239/j.cnki.0468-155x.2023.05.011
- Liu, Y., Li, J., Sun, C., Wang, X., Tian, P., Chen, L., et al. (2023). Thirty-year changes of the coastlines, wetlands, and ecosystem services in the Asia major deltas. *J. Environ. Manage* 326, 116675. doi: 10.1016/j.jenvman.2022.116675
- Liu, G. Y., and Zhang, X. L. (2001). Environmental geological problems and sustainable economic development of oil and gas resources in the Yellow River delta. *Shanghai Geology* B12, 36–38.
- Liu, X., Zhang, H., Zheng, J., Guo, L., Jia, Y., Bian, C., et al. (2020). Critical role of wave-seabed interactions in the extensive erosion of yellow river estuarine sediments. *Mar. Geology* 426, 106208. doi: 10.1016/j.margeo.2020.106208
- Liu, X. L., Zheng, J. W., Zhang, H., Zhang, S. T., Liu, B. H., Shan, H. X., et al. (2018). Sediment critical shear stress and geotechnical properties along the modern yellow river delta, China. *Mar. Georesources Geotechnology* 36, 875–888. doi: 10.1080/1064119X.2017.1393477
- Ma, Y. Y. (2008). *Evolution of modern Yellow River Delta coastal environment*. [PhD Thesis] (Shandong: Ocean University of China).
- Ma, Z. C., Chen, S., and Zhang, Q. (2022). Spatiotemporal analysis and prediction of erosion of intertidal sediments in the sunda strait based on DSAS model and GEE long time series images. *Resour. Environ. Eng* 36, 836–842. doi: 10.16536/j.cnki.issn.1671-1211.2022.06.016
- Maier, M.-S., Teodoru, C. R., and Wehrli, B. (2021). Spatio-temporal variations in lateral and atmospheric carbon fluxes from the Danube Delta. *Biogeosciences* 18, 1417–1437. doi: 10.5194/bg-18-1417-2021
- McLaren, K., Sedman, J., McIntyre, K., and Prospere, K. (2024). Long-term spatial pattern predictors (Historically low rainfall, benthic topography, and hurricanes) of seagrass cover change, (1984 to 2021) in a Jamaican Marine Protected Area. *Remote Sens* 16, 1247. doi: 10.3390/rs16071247
- Meng, X., Jia, Y., Shan, H., Yang, Z., and Zheng, J. (2012). An experimental study on erodibility of intertidal sediments in the yellow river delta. *Int. J. Sediment Res* 27, 240–249. doi: 10.1016/S1001-6279(12)60032-8
- Moftakhari, H. R., Salvadori, G., AghaKouchak, A., Sanders, B. F., and Matthew, R. A. (2017). Compounding effects of sea level rise and fluvial flooding. *Proc. Natl. Acad. Sci. U.S.A.* 1149785, –9790. doi: 10.1073/pnas.1620325114
- Nassar, K., Mahmood, W. E., Fath, H., Masria, A., Nadaoka, K., and Negm, A. (2019). Shoreline change detection using DSAS technique: case of north sinai coast, Egypt. *Mar. Georesources Geotechnology* 37, 81–95. doi: 10.1080/1064119X.2018.1448912
- Nienhuis, J. H., and Van De Wal, R. S. W. (2021). Projections of global delta land loss from sea-level rise in the 21st century. *Geophysical Res. Lett.* 48, e2021GL093368. doi: 10.1029/2021GL093368
- Nguyen, T. C., Schwarzer, K., and Ricklefs, K. (2023). Water-level changes and subsidence rates along the Saigon-Dong Nai River Estuary and the East Sea coastline of the Mekong Delta. *Estuarine Coast. Shelf Sci* 283, 108259. doi: 10.1016/j.ecss.2023.108259
- Ning, R. R., Wang, D., and Tian, X. P. (2023). Analysis of ground settlement in the Yellow River Delta and projection of seawater inundation. *Adv. Earth Sci* 38, 296–308. doi: 10.11867/j.issn.1001-8166.2023.006
- Paul, S., Chowdhury, S., and Chaudhuri, S. (2022). Analysing the trend of beach-dune erosion in digha coastal tract in response to nearshore wave processes and coastal protection structures. *Regional Stud. Mar. Sci* 52, 102243. doi: 10.1016/j.rsma.2022.102243
- Qi, H., Cai, F., Lei, G., Cao, H., and Shi, F. (2010). The response of three main beach types to tropical storms in South China. *Mar. Geology* 275, 244–254. doi: 10.1016/j.margeo.2010.06.005
- Rateb, A., and Abotalib, A. Z. (2020). Inferencing the land subsidence in the Nile Delta using Sentinel-1 satellites and GPS between 2015 and 2019. *Sci. Total Environ* 729, 138868. doi: 10.1016/j.scitotenv.2020.138868
- Ren, Z. H. (2023). *Research on the evolution of estuarine geomorphology in the Diaokou sub-delta of Yellow River since 1964*. [master's thesis] (Shandong: Ludong University).
- Ren, T., Gong, W., Gao, L., and Zhao, F. (2024). Understanding land subsidence in the Pearl River Delta region of China based on InSAR observations. *Eng. Geology* 339, 107646. doi: 10.1016/j.enggeo.2024.107646
- Shen, K. M., Li, A. L., and Jiang, Y. B. (2020). Time-space velocity analysis of coastline based on digital shoreline analysis system: A case study of the Haizhou Bay. *Haiyang Xuebao* 42, 177–127. doi: 10.3969/j.issn.0253-4193.2020.05.011
- Stanley, D. J. (1990). Recent subsidence and northeast tilting of the Nile delta, Egypt. *Mar. Geology* 94, 147–154. doi: 10.1016/0025-3227(90)90108-V
- Stănică, A., Dan, S., Jiménez, J. A., and Ungureanu, G. V. (2011). Dealing with erosion along the danube delta coast. the CONSCIENCE experience towards a sustainable coastline management. *Ocean Coast. Manage.* 54898, –906. doi: 10.1016/j.ocecoaman.2011.06.006
- Stănică, A., and Panin, N. (2009). Present evolution and future predictions for the deltaic coastal zone between the sulina and sf. gheorghe danube river mouths (Romania). *Geomorphology* 107, 41–46. doi: 10.1016/j.geomorph.2007.04.041

- Sun, W., Chen, C., Liu, W., Yang, G., Meng, X., Wang, L., et al. (2023). Coastline extraction using remote sensing: a review. *GIScience Remote Sens* 60, 2243671. doi: 10.1080/15481603.2023.2243671
- Sun, H. Q., Cui, B. L., and Jiang, D. J. (2024). Dynamics and driving factors of carbon storage in the Yellow River Delta from 1980 to 2020. *Pearl River*. 45, 36–46.
- Syvitski, J. P. M., Kettner, A. J., Overeem, I., Hutton, E. W. H., Hannon, M. T., Brakenridge, G. R., et al. (2009). Sinking deltas due to human activities. *Nat. Geosci* 2, 681–686. doi: 10.1038/ngeo629
- Tang, M., Xu, Y. J., Xu, W., Wang, B., and Cheng, H. (2021). Three-decadal erosion and deposition of channel bed in the Lower Atchafalaya River, the largest distributary of the Mississippi River. *Geomorphology* 380, 107638. doi: 10.1016/j.geomorph.2021.107638
- Teatini, P., Tosi, L., and Strozzi, T. (2011). Quantitative evidence that compaction of Holocene sediments drives the present land subsidence of the Po Delta, Italy. *J. Geophys. Res* 116, B08407. doi: 10.1029/2010JB008122
- Thakur, S., Mondal, I., Bar, S., Nandi, S., Ghosh, P. B., Das, P., et al. (2021). Shoreline changes and its impact on the mangrove ecosystems of some islands of Indian sundarbans, north-east coast of India. *J. Cleaner Production* 284, 124764. doi: 10.1016/j.jclepro.2020.124764
- The Geodetic Survey Brigade For Earthquake Research, National Seismological Bureau (1977). Ground surface deformation of the haicheng earthquake of magnitude 7.3. *Acta GEOPHYSICA Sin* 04, 251–263.
- Törnqvist, T. E., Wallace, D. J., Storms, J. E. A., Wallinga, J., Van Dam, R. L., Blaauw, M., et al. (2008). Mississippi Delta subsidence primarily caused by compaction of Holocene strata. *Nat. Geosci* 1, 173–176. doi: 10.1038/ngeo129
- Turner, R. E., Swenson, E. M., Milan, C. S., and Lee, J. M. (2007). Hurricane signals in salt marsh sediments: Inorganic sources and soil volume. *Limnology Oceanography* 52, 1231–1238. doi: 10.4319/lo.2007.52.3.1231
- Wang, X. Y. (2022). *Historical evolution analysis of the Yellow River Delta based on typical tail channel sedimentary column and shoreline change. [master's thesis]* (Shandong: Yantai University).
- Wang, X.-L., Feng, A.-Q., Hou, X.-Y., Chao, Q.-C., Song, B.-Y., Liu, Y.-B., et al. (2024). Compound extreme inundation risk of coastal wetlands caused by climate change and anthropogenic activities in the Yellow River Delta, China. *Adv. Climate Change Res* 15, 134–147. doi: 10.1016/j.accre.2024.01.010
- Wang, J., Wang, J., Zhang, Z., Li, Z., Zhang, Z., Zhao, D., et al. (2020). Shifts in the bacterial population and ecosystem functions in response to vegetation in the yellow river delta wetlands. *mSystems* 5. doi: 10.1128/msystems.00412-20
- Wang, H., Wright, T. J., Yu, Y., Lin, H., Jiang, L., Li, C., et al. (2012). InSAR reveals coastal subsidence in the Pearl River Delta, China. *Coast. subsidence PRD. Geophysical J. Int.* 191, 1119–1128. doi: 10.1111/j.1365-246X.2012.05687.x
- Wang, H., Wu, X., Bi, N., Li, S., Yuan, P., Wang, A., et al. (2017). Impacts of the dam-orientated water-sediment regulation scheme on the lower reaches and delta of the Yellow River (Huanghe): A review. *Global Planetary Change* 157, 93–113. doi: 10.1016/j.gloplacha.2017.08.005
- Wang, L., Xu, H. Q., and Li, S. (2005). Dynamic monitoring of the shoreline changes in xiamen island with its surrounding areas of SE China using remote sensing technology. *Remote Sens. Technol. Appl* 04, 404–410.
- Wang, Q., Zeng, L., Zhan, C., Liu, X., Wang, L., Cheng, S., et al. (2022). Geomorphologic evolution of the shallow-buried abandoned Yellow River delta during the last 2000 years. *Front. Mar. Sci* 9. doi: 10.3389/fmars.2022.1073961
- Williams, H. F. L. (2009). Stratigraphy, sedimentology, and microfossil content of hurricane rita storm surge deposits in southwest louisiana. *J. Coast. Res* 254, 1041–1051. doi: 10.2112/08-1038.1
- Wu, G. D. (2017). *Characteristics and disaster risk analysis of storm surge in the Yellow River Delta. [master's thesis]* (Shandong: First Institution of Oceanography, MNR).
- Wu, Y., Hong, T., Meng, L., Xiao, L., Li, Y., and Bi, X. (2023). Identification of wetland conservation and restoration priorities in regions of oil extraction in the Yellow River Delta using circuit theory modelling. *Ecol. Indic* 154, 110621. doi: 10.1016/j.ecolind.2023.110621
- Wu, X., Liu, C., and Wu, G. (2018). Spatial-temporal analysis and stability investigation of coastline changes: A case study in shenzhen, China. *IEEE J. Sel. Top. Appl. Earth Observations Remote Sens* 11, 45–56. doi: 10.1109/JSTARS.2017.2755444
- Wu, B. S., Zheng, S., and Wang, K. R. (2021). Processes and calculation method of tail channel length in the Yellow River Estuary. *J. Sediment Res* 46, 75–80. doi: 10.16239/k.cnki.0468-155x.2021.04.012
- Xia, J., Luan, G., Zhao, F., Peng, Z., Song, L., Tan, S., et al. (2021). Exploring the spatial-temporal analysis of coastline changes using place name information on hainan island, China. *IJGI* 10, 609. doi: 10.3390/ijgi10090609
- Xiao, D. N., Han, M. K., and Li, X. W. (2003). Sea level rising around Bohai Sea and deltaic wetlands protections. *Quaternary Sci* 23, 237–246.
- Xing, G., Wang, H., Yang, Z., and Bi, N. (2016). Spatial and temporal variation in erosion and accumulation of the subaqueous yellow river delta, (1976–2004). *J. Coast. Res* 74, 32–47. doi: 10.2112/SI74-004.1
- Xiong, F., and Zhu, W. Y. (2007). Land deformation monitoring by GPS in the yangtze delta and the measurements analysis. *Chin. J. Geophysics* 50, 1501–1514. doi: 10.1002/cjg2.1170
- Xu, C. L., Chen, S. L., and Chen, J. Q. (2018). Evolution mode of channel bifurcation delta system at the yellow river delta estuary under the new situation. *Coast. Eng* 37, 35–43. doi: 10.3969/j.issn.1002-3682.2018.04.005
- Xu, L., Li, J., Li, W., Zhao, S., Yuan, Q., and Wang, M. (2014). Progress in impact of human activities on coastal resource and environment. *J. Nanjing Normal Univ. (Natural Sci. Edition)* 3, 124–131.
- Xu, J., Zhang, Z., Zhao, X., Wen, Q., Zuo, L., Wang, X., et al. (2014). Spatial and temporal variations of coastlines in northern China, (2000–2012). *J. Geogr. Sci* 24, 18–32. doi: 10.1007/s11442-014-1070-x
- Yang, S. L., Fan, J. Q., Shi, B. W., Bouma, T. J., Xu, K. H., Yang, H. F., et al. (2019). Remote impacts of typhoons on the hydrodynamics, sediment transport and bed stability of an intertidal wetland in the Yangtze Delta. *J. Hydrology* 575, 755–766. doi: 10.1016/j.jhydrol.2019.05.077
- Yao, Q., Cohen, M. C. L., Liu, K., De Souza, A. V., and Rodrigues, E. (2022). Nature versus humans in coastal environmental change: assessing the impacts of hurricanes zeta and ida in the context of beach nourishment projects in the mississippi river delta. *Remote Sens* 14, 2598. doi: 10.3390/rs14112598
- Ye, T., Chen, A., Hou, M., Niu, C., and Wang, Q. (2021). Characteristic of the Bodong segment of the Tanlu Fault Zone, Bohai sea area, eastern China: Implications for hydrocarbon exploration and regional tectonic evolution. *J. Petroleum Sci. Eng* 201, 108478. doi: 10.1016/j.petrol.2021.108478
- Ye, X. M., Ding, J., and Xu, Y. (2016). On the changes of the coastline in bohai bay during the last 30 years. *Ocean Dev. Manage* 33, 56–62. doi: 10.20016/j.cnki.hykyjgl.2016.02.011
- Yi, W. H. (2011). *Representative coastal erosion processes and controlling factors. [Master Thesis]* (Shandong: Ocean University of China).
- Yu, X., Wang, W. Z., and Li, Y. (2016). Processes of the Yellow River Estuary since operation of the Xiaolangdi Reservoir. *J. Sediment Res* 06, 8–11. doi: 10.16239/j.cnki.0468-155x.2016.06.002
- Zhan, C., Wang, Q., Cheng, S., Zeng, L., Yu, J., Dong, C., et al. (2023). Investigating the evolution of landscape patterns in historical subdeltas and coastal wetlands in the Yellow River Delta over the last 30 years: A geo-informatics approach. *Front. Mar. Sci* 10. doi: 10.3389/fmars.2023.1115720
- Zhan, C., Wang, Q., Cui, B., Zeng, L., Dong, C., Li, X., et al. (2020). The morphodynamic difference in the western and southern coasts of Laizhou Bay: Responses to the Yellow River Estuary evolution in the recent 60 years. *Global Planetary Change* 187, 103138. doi: 10.1016/j.gloplacha.2020.103138
- Zhang, J. Z. (2015). *Monitoring of Land Subsidence in Morden Yellow River Delta Based on InSAR Time Series Analysis Techniques and the Analysis of its Typical Influence Factors. [PhD thesis]* (Shandong: Ocean University of China).
- Zhang, X. (2021). *Analysis of coastline changes in shandong peninsula and typical regions of China based on remote sensing images. [Master thesis]* (Shandong: Qingdao University).
- Zhang, Z. H., and Hu, C. H. (2007). Variation of the processes of flow and sediment and its effect on epeirogenesis of seacoast in the Yellow River estuary. *Adv. Water Sci* 03, 336–341. doi: 10.14042/j.cnki.32.1309.2007.03.004
- Zhang, B., Liu, G. Y., and Fan, L. Q. (2004). Environmental problem and its prevention countermeasures of underground water in south of Huanghe Delta. *Shandong Land Resour* 20, 51–54.
- Zhang, Y., Lou, Y. F., and Huang, H. J. (2022). Correlating severe land subsidence and confined brine aquifer compaction in the Yellow River Delta, China, with Sentinel-A/1B satellite images. *Mar. Georesources Geotechnology* 41, 927–934. doi: 10.1080/1064119X.2022.2109537
- Zhang, B., Wang, R., Deng, Y., Ma, P., Lin, H., and Wang, J. (2019). Mapping the Yellow River Delta land subsidence with multitemporal SAR interferometry by exploiting both persistent and distributed scatterers. *ISPRS J. Photogrammetry Remote Sens* 148, 157–173. doi: 10.1016/j.isprsjprs.2018.12.008
- Zheng, J., Jia, Y., and Liu, X. (2015). Field measurement of sediment critical shear stress in the modern Yellow River Delta. *Haiyang Xuebao* 37, 86–98. doi: 10.3969/j.issn.0253-4193.2015.03.009
- Zhou, X., Wang, J., Zheng, F., Wang, H., and Yang, H. (2023). An overview of coastline extraction from remote sensing data. *Remote Sens* 15, 4865. doi: 10.3390/rs15194865
- Zhu, Y., Lu, L., Li, Z., Wang, S., Yao, Y., Wu, W., et al. (2024). Monitoring land use changes in the yellow river delta using multi-temporal remote sensing data and machine learning from 2000 to 2020. *Remote Sens* 16, 1946. doi: 10.3390/rs16111946
- Zuo, F. J., Cao, Y., and Fan, Z. (2024). Research on the stability of river mouth shoreline in the Yellow River Delta from 1996 to 2022. *Mar Sci Bull* 43, 426.